Science of the Total Environment 892 (2023) 164702

Contents lists available at ScienceDirect

Science of the Total Environment

journal homepage: www.elsevier.com/locate/scitotenv

Optical properties and molecular composition of wintertime atmospheric water-soluble organic carbon in different coastal cities of eastern China

Haibiao Chen [a], Caiqing Yan [a,b,*], Qinglong Fu [c], Xinfeng Wang [a], Jiao Tang [d], Bin Jiang [d], Honglei Sun [a], Tiancheng Luan [a], Qiaoyun Yang [e], Qianbiao Zhao [f], Jun Li [d], Gan Zhang [d], Mei Zheng [g], Xuehua Zhou [a], Bing Chen [a], Lin Du [a], Ruizhi Zhou [a], Taomeizi Zhou [a], Likun Xue [a]

[a] Environment Research Institute, Shandong University, Qingdao 266237, China
[b] State Environmental Protection Key Laboratory of Formation and Prevention of the Urban Air Complex, Shanghai Academy of Environmental Sciences, Shanghai 200233, China
[c] School of Environmental Studies, China University of Geosciences, Wuhan 430074, China
[d] State Key Laboratory of Organic Geochemistry and Guangdong Key Laboratory of Environmental Protection and Resources Utilization, Guangzhou Institute of Geochemistry, Chinese Academy of Sciences, Guangzhou 510640, China
[e] Department of Occupational and Environmental Health, School of Public Health, Tianjin Medical University, Tianjin 300070, China
[f] Academy of Environmental Planning & Design, Co., Ltd. Nanjing University, Nanjing 210093, China
[g] SKL-ESPC and BIC-ESAT, College of Environmental Sciences and Engineering, Peking University, Beijing 100871, China

HIGHLIGHTS

- Fluorophores were mainly related to less-oxygenated HULIS and primary emissions.
- Continental-influenced WSOC showed higher light absorption coefficient and efficiency.
- Continental-influenced WSOC had relatively more unsaturated and aromatic molecules.
- More organohalogen compounds were identified in marine air masses influenced WSOC.

GRAPHICAL ABSTRACT

Figure. Discrepancies of optical properties and molecular compositions between Con-influenced and Mar-influenced WSOC.

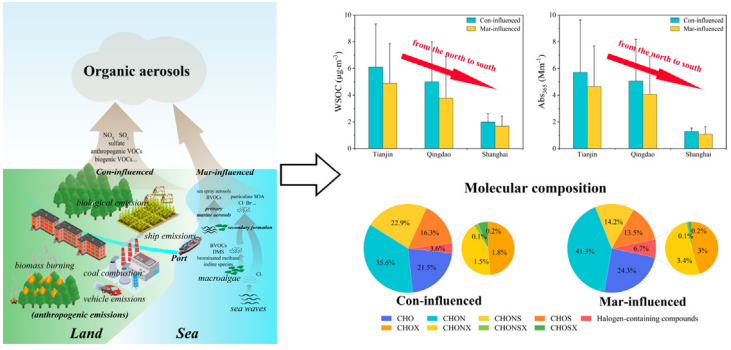

ARTICLE INFO

Editor: Jianmin Chen

Keywords:
WSOC
Light-absorbing properties
Fluorophores
FT-ICR MS
Marine air masses
Organohalogen compounds

ABSTRACT

To evaluate the optical properties and molecular composition of water-soluble organic carbon (WSOC) in the atmosphere of coastal cities, particle samples were collected in Tianjin, Qingdao and Shanghai, three coastal cities in eastern China. Subsequent analysis by ultraviolet visible and fluorescence spectrometer and electrospray ionization Fourier transform ion cyclotron resonance mass spectrometry were performed. The results showed that the concentration levels and light absorption ability of WSOC decreased from the north to south cities, ranking as Tianjin > Qingdao > Shanghai. Three major fluorescent components including less-oxygenated humic-like substances (52–60 %), highly-oxygenated humic-like substances (15–31 %) and protein-like substances (17–31 %) were identified in WSOC based on the fluorescence spectroscopy and parallel factor analysis, which might be closely related to anthropogenic emissions and continental sources as well as secondary formation processes. Five subgroups of molecular components were further identified in WSOC, including the predominant CHON compounds (35–43 %), sulfur-containing compounds (i.e., CHONS and CHOS compounds, 24–43 %), CHO compounds (20–26 %) and halogen-containing compounds (1–7 %). Compared to marine air masses influenced samples, WSOC affected by continental air masses

* Corresponding author at: Environment Research Institute, Shandong University, Qingdao 266237, China.
E-mail address: cyan0325@sdu.edu.cn (C. Yan).

http://dx.doi.org/10.1016/j.scitotenv.2023.164702
Received 15 February 2023; Received in revised form 26 May 2023; Accepted 4 June 2023
Available online 9 June 2023

exhibited higher light absorption coefficients and generally had a higher degree of aromaticity and unsaturation, as well as contained more molecular formulas of WSOC, especially enriched with sulfur-containing compounds. In contrast, relatively more abundant halogen-containing compounds were identified in the marine air masses influenced samples. Overall, this study provided new insights into the light-absorbing and chemical properties of WSOC in coastal cities, especially under the influences of continental and marine air masses.

1. Introduction

Water-soluble organic carbon (WSOC) is a critical constituent of atmospheric organic aerosols, which accounts for a substantial fraction (20–80 %) of atmospheric organic aerosols (Du et al., 2014a; Kirillova et al., 2014a). WSOC can be originated from primary emissions (e.g., biomass burning and coal combustion) (Hecobian et al., 2010; Olson et al., 2015; Yan et al., 2015) or secondary formation through the oxidation of atmospheric volatile organic compounds (VOCs) (He et al., 2021; Lin et al., 2015; Weber et al., 2007). Previous studies have shown that WSOC could enhance the hygroscopicity of particles and influence the activity of cloud condensation nuclei (CCN), and has a significant impact on the global climate (Fuzzi et al., 2001; Seinfeld et al., 2016). In the past decades, special attention has been paid to the physicochemical properties of WSOC, especially for the components with strong light-absorption ability, which are defined as brown carbon (BrC) (Andreae and Gelencsér, 2006). The sources and light absorption properties of water-soluble brown carbon (WS-BrC) have been found to have significant temporal and spatial variations (Du et al., 2014b; Hecobian et al., 2010; Kirillova et al., 2014b; Yuan et al., 2020). A comprehensive understanding of the optical properties, sources and molecular compositions of WSOC in different regions is necessary to assess their climate effects. However, previous studies are mainly focused on the inland urban areas especially some megacities, while researches on the WSOC in coastal regions are still scarce.

Located in the junction of land and ocean, atmospheric organic aerosols in coastal cities could be affected by continental emissions and sea breezes, and may have significant regional characteristics (Bai et al., 2020; Ding et al., 2004; Kuang et al., 2015; Tolis et al., 2015). Aerosols in coastal cities may enrich with sea spray-derived organic matters when influenced by marine biological activities (Bao et al., 2018). For example, low molecular weight organic molecular compositions (e.g., n-alkanes, fatty acids) have been observed in the coastal atmosphere under the influence of sea breezes due to the transport of marine organic matters (Fan et al., 2020). In addition, a recent study indicated that WSOC influenced by marine air masses was more enriched with saturated and lower oxidation level primary marine biological compounds (Mo et al., 2022). Furthermore, ship emission may be a non-negligible contributor to the light-absorbing component of WSOC in port cities (Bai et al., 2020; Yu et al., 2018). Halogen and dimethyl sulfide (DMS) or isoprene emitted from the ocean can affect the secondary formation of organic aerosols in the atmosphere by changing the concentration levels of OH, HO_2, NO_3 and O_3 in the coastal atmosphere (Gantt et al., 2010; Muñiz-Unamunzaga et al., 2018). The oxidation of VOCs (e.g., polycyclic aromatic hydrocarbons, furan or monoterpenes) by chlorine atom could also be an important source of organic aerosols in coastal regions (Cabanas et al., 2005; Cai and Griffin, 2006; Tanaka et al., 2003; Wang et al., 2005). However, most of the current organic aerosol related studies in coastal cities were mainly focused on water-soluble ions, small molecule organic acids (e.g., dicarboxylic acids), or formation mechanisms of marine secondary organic aerosols (Bikkina et al., 2017; Tolis et al., 2015; Zhou et al., 2018).

So far, the knowledge about the optical properties and molecular composition of WSOC in coastal regions is still very limited. In particular, the measurement and research of organochloride in particulate matter in coastal areas are still very few. In this study, fine particulate matter ($PM_{2.5}$) samples were collected in three typical coastal port cities in eastern China in winter. The primary objectives of this study include (1) investigating the similarities and differences of optical properties and molecular composition of WSOC in different coastal cities, and (2) exploring the discrepancies of chemical properties of WSOC under the influences of continental and marine air masses.

2. Materials and methods

2.1. Sample collection

$PM_{2.5}$ samples were collected in Tianjin (TJ), Qingdao (QD) and Shanghai (SH) (Fig. 1). These three cities are important coastal and port cities in eastern China, which may be affected by continental and oceanic air masses as well as ship emissions. Tianjin locates in the Beijing-Tianjin-Hebei region, and is adjacent to the Bohai Sea of China. Qingdao is situated on the heavily polluted Shandong Peninsula, adjacent to the Yellow Sea and downwind of the North China Plain. And Shanghai locates in the Yangtze River Delta region, bordering on the East China Sea. These three cities can be representative of coastal cities in the three of the typical regions in China, and in northern and southern China, respectively, with differences in ambient temperatures and anthropogenic and biogenic source emissions. Therefore, the selection of these three cities provides an opportunity to better understand the optical properties and molecular composition of atmospheric water-soluble organic aerosols under the influence of different air masses and emission sources.

The TJ site has been described in our previous study (Zhou et al., 2023). Briefly, it was located on the campus of Tianjin Medical University (39.11°N, 117.19°E) and surrounded by residential buildings. The QD site was located on the rooftop of one teaching building on the campus of Qingdao Research Institute of Northwestern Polytechnical University (36.35°N, 120.67°E), which was mainly surrounded by villages and residential buildings. The SH site was situated on the rooftop of the building of the Shanghai Environmental Monitoring Center (31.17°N, 121.44°E), locating in a mixed district of residential, commercial and teaching areas, and there was a main traffic road about 300 m away. A mid-volume air sampler (TH-150A, Wuhan Tianhong, China) was used to collect $PM_{2.5}$ samples on quartz-fiber filters (90 mm; Whatman, grade QMA 9.0CM, USA) at a flow rate of 100 $L{\cdot}min^{-1}$. Daily $PM_{2.5}$ samples were collected from 29 November

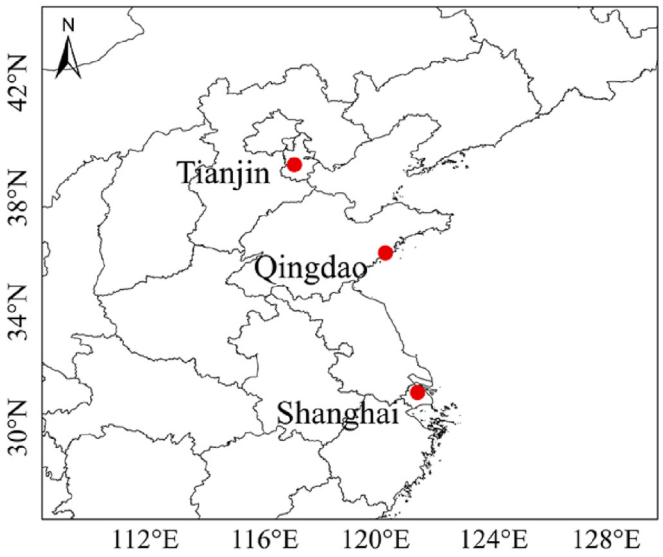

Fig. 1. The location map of the three sampling sites in this study.

2019 to 6 January 2020 in TJ and from 12 November to 25 December 2019 in QD, respectively. The sampling duration for each sample was 23.5 h, with the collection time starting at 8:00 am and stopping at 7:30 am on the next day. Samples in SH were collected on quartz-fiber filters (8 × 10 in.; Whatman, grade QMA 8 × 10IN, USA) using a high-volume air sampler (Tisch Environment, USA) at a flow rate of 1.13 $m^3 \cdot min^{-1}$ from 12:00 pm to 10:00 am the next day (22 h) during December 1–28 of 2020. All quartz-fiber filters were prebaked at 550 °C for 5.5 h before sampling to remove potential organic matters. After sampling, the filter samples were wrapped in prebaked aluminum foils and stored under −20 °C in the refrigerator until further analysis.

2.2. Chemical analysis

A punch of 1.5 cm^2 subsample taken from each filter sample was analyzed by the thermal optical transmittance (TOT) carbon analyzer (Sunset Laboratory, Inc., Tigard, OR, USA) following the National Institute for Occupational Safety and Health (NIOSH) protocol to determine the concentrations of organic carbon (OC) and elemental carbon (EC). Sucrose standard solution was applied to test the status of the instrument before and during the measurement, and OC and EC concentrations were corrected by a standard curve to ensure the accuracy and reliability of the results. Besides, an area of 6 cm^2 cut from each sample was extracted by ultra-sonication for 30 min with ultrapure water (>18.2 MΩ·cm, 25 °C, Direct-Q, Millipore). The water extracts were then filtered with a PTFE pore syringe filter (0.45 μm; Pall, USA) to remove insoluble materials. A portion of the extracts was used to quantify the WSOC concentrations by an Elementar vario TOC cube elemental analyzer (Elementar, Germany).

2.3. Light absorption and fluorescence analysis

Light absorption spectrum of WSOC was recorded by a spectrophotometer (TIDAS®S 300 UV/VIS 1972 DH, J&M, Germany) coupled with a 1 m long-path liquid waveguide capillary cell (LWCC-3100, World Precision Instruments Inc., USA) over the wavelength range of 250–700 nm with the scanning interval of 1 nm. Ultrapure water was used for blank correction during the measurements. The light absorption coefficient (Abs_λ, Mm^{-1}) of WSOC at the wavelength λ was calculated as follows,

$$Abs_\lambda = (A_\lambda - A_{700}) \times \frac{V_l}{V_a \times L} \times \ln(10) \quad (1)$$

where V_l (mL) is the volume of the filtered extract, V_a (m^3) is the air volume corresponding to the extracted filter area, and L is the optical path length (1 m here). A_λ is the absorbance at wavelength λ measured by the spectrophotometer. In this study, Abs_{365} was chosen as a proxy for the absorbance of WS-BrC to exclude the interferences of other substances (e.g., nitrate, etc.) (Hecobian et al., 2010). A_{700} was chosen to reduce the effects of baseline drift during the measurement and ln (10) was used to convert the absorption coefficient from log base 10 to natural logarithm.

Mass absorption efficiency (MAE, $m^2 \cdot g^{-1}$) was widely used to characterize the light absorption ability of WSOC, and was calculated as follows,

$$MAE_\lambda = \frac{Abs_\lambda}{C_{WSOC}} \quad (2)$$

where C_{WSOC} ($\mu g \cdot m^{-3}$) represents WSOC mass concentration.

The spectral dependence of light absorption for WSOC could be described by the Ångström absorption exponent (AAE), which was obtained by a linear regression fitting of the light absorption over the wavelengths of 330–400 nm according to the Eq. (3),

$$AAE = -\frac{\ln(Abs(\lambda_1)/Abs(\lambda_2))}{\ln(\lambda_1/\lambda_2)} \quad (3)$$

About 3 mL of the aqueous filter extracts were used for fluorescence measurement using a fluorescence and absorbance spectrometer (Duetta™, Horiba Scientific, Japan). Excitation-emission matrix (EEM) spectrum with excitation (Ex) and emission (Em) wavelength range of 250–600 nm was obtained, with scanning intervals set to 5 and 2 nm and slit width fixed at 5 nm. Parallel factor analysis (PARAFAC) with the non-negativity constraint of ultrapure-water-corrected EEM data was performed using the DOMFluor toolbox for MATLAB R2020a to identify the potential chromophore components at the three sites (Stedmon and Bro, 2008). Besides, fluorescence indices were calculated to provide source information on atmospheric organic aerosols. The fluorescence index (FI, the ratio of emission intensity of 450 nm to 500 nm under the Ex of 370 nm), biological index (BIX, the ratio of emission intensity of 380 nm to 430 nm under the Ex of 310 nm) and humidification index (HIX, the ratio of the integrated emission intensity in the ranges of 435–480 nm to 300–345 nm under the Ex of 255 nm) were determined according to the following equations (Wu et al., 2021), respectively,

$$FI = \frac{F(E_x = 370\ nm, E_m = 450\ nm)}{F(E_x = 370\ nm, E_m = 500\ nm)} \quad (4)$$

$$BIX = \frac{F(E_x = 310\ nm, E_m = 380\ nm)}{F(E_x = 310\ nm, E_m = 430\ nm)} \quad (5)$$

$$HIX = \frac{F(E_x = 255\ nm, E_m = 435 - 480\ nm)}{F(E_x = 255\ nm, E_m = 300 - 345\ nm)} \quad (6)$$

2.4. Molecular composition analysis and related data treatment

The 48-h backward air mass trajectory was calculated (at 500 m above ground level) for every single day with the national oceanic and atmospheric administration (NOAA) Hybrid Single-particle Lagrangian Integrated Trajectory (HYSPLIT) model (https://www.ready.noaa.gov/HYSPLIT_traj.php) (Stein et al., 2015). Cluster analysis implied that air masses arriving at the sampling sites including continental and marine air masses (Fig. S1), with 16–42 % of air masses from marine. Samples affected by continental air masses (Con-influenced) and marine air masses (Mar-influenced) were identified and selected at each site for further Fourier transform ion cyclotron resonance mass spectrometry (FT-ICR MS) analysis (Fig. S2). A subsample with an area of 15.9 cm^2 was punched from the selected sample and was extracted with 20 mL ultrapure water using an ultrasonic bath for 30 min and then filtered by a 0.22 μm PTFE membrane (Anpel, China) to remove insoluble particles. The extraction was further adjusted to pH = 2 by adding HCl (1 M) and then passed through a preconditioned solid-phase extraction (SPE) cartridge (Oasis HLB, 30 μm, 200 mg/cartridge; Waters, Milford, MA, USA). Organic compounds retained on the SPE cartridge were further eluted with methanol containing 2 % ammonia (*v*/v, 6 mL) and dried under a gentle high-purity nitrogen (N_2) stream. After that, the dried-eluate was re-dissolved in methanol and then analyzed by the FT-ICR MS.

In this study, a solariX XR FT-ICR MS (Bruker Daltonics GmbH, Bremen, Germany) equipped with a 9.4 T refrigerated actively shielded superconducting magnet (Bruker Biospin, Wissembourg, France) and a ParaCell analyzer cell (Gamry Instruments, Warminster, PA, USA) was adopted. More detailed description of the instrument and measuring conditions could be found in Mo et al. (2018). Briefly, the samples were ionized in the negative ion mode using the electrospray ionization ion source (ESI-) (Bruker Daltonics). The ion accumulation time was set to 0.6 s, and a total of 100 continuous 4 M data points of FT-ICR transients were added to enhance the signal-to-noise (S/N) ratio. The detection mass range was set to *m/z* 100–800 and the mass spectra were calibrated externally with arginine clusters in the negative ion mode using a linear calibration. The final spectrum was internally recalibrated with typical O_3 class species peaks using quadratic calibration in DataAnalysis ver. 5.0 (Bruker Daltonics). A typical mass-resolving power (m/Δm50%, in which Δm50% is the magnitude of the mass spectral peak full width at half-maximum peak

height) > 450,000 at *m/z* 319 with <0.2 ppm absolute mass error was achieved.

An algorithm for D-labeled UHR-MS spectra (FTMSDeu) developed by Fu et al. (2022) was used to calculate all the mathematically possible formulas for all ions with S/*N* ≥ 10 and mass tolerance of ±1 ppm. Each of the detected molecular formulas ($C_cH_hO_oN_nS_sCl_jBr_kI_l$) contains certain elements, including carbon (C), hydrogen (H), oxygen (O), nitrogen (N), sulfur (S), chlorine (Cl), bromine (Br), and iodine (I). The calculator was set as $C_{1\text{-}50}H_{1\text{-}60}O_{1\text{-}15}N_{1\text{-}5}S_{1\text{-}3}Cl_{1\text{-}3}Br_{1\text{-}2}I_{1\text{-}2}$, and the identified formulas containing isotopes (i.e., ^{13}C, ^{18}O, ^{34}S, ^{37}Cl, ^{81}Br) were not discussed. To rule out the compounds that were unlikely to exist in nature, the H/C, O/C, N/C and S/C ratios were limited to 0.3–3.0, 0–3.0, 0–0.5 and 0–2.0, respectively. Besides, all the calculated formulas that disobey the nitrogen rule were excluded. Finally, the identified molecular formulas were apportioned to five major groups, including CHO (containing carbon, hydrogen and oxygen atoms, the other groups are defined analogously), CHON, CHONS, CHOS and halogen-containing compounds (HCCs, including CHOX, CHONX, CHONSX, and CHOSX, where X represents halogen atoms including Cl, Br and I). Therein, HCCs were further classified into thirteen subgroups (i.e., CHOBr, CHOCl, CHOClBr, CHOI, CHONBr, CHONCl, CHONClI, CHONI, CHONSBr, CHONSCl, CHOSBr, CHOSCl and CHOSI) based on C, H, O, N, S, and halogen atoms (Cl, Br, and I).

The double-bond equivalents (DBE) and the modified aromaticity index (AI_{mod}) of compounds were calculated as follows (Fu et al., 2022),

$$DBE = 1 + \frac{2c - (h + j + k + l) + n}{2} \tag{7}$$

$$AI_{mod} = \frac{1 + c - 0.5o - s - 0.5\,(h + n + j + k + l)}{c - 0.5o - n - s} \tag{8}$$

where c, h, o, n, s, j, k, and l refer to the stoichiometric number of C, H, O, N, S, Cl, Br, and I atoms in per formula. And if $AI_{mod} < 0$, then it was regarded as $AI_{mod} = 0$.

The molecular parameters (MP) were assessed with relative intensity weight by the following equation,

$$MP_{i,w} = \frac{\Sigma(Int_i \times MP_i)}{\Sigma Int_i} \tag{9}$$

where MP and Int are the molecular parameters (e.g., molecular weight, O/C, H/C, DBE, and AI_{mod}, etc.) and the intensity of formula i, respectively.

For $CHOS_1$ compounds, an alternative notation was introduced using O* (defined as x - 3, where x represents the number of O atoms) (Tao et al., 2014). The new aromaticity index (AI*) was calculated by the following equation (Su et al., 2022),

$$AI^* = (DBE - O^*)/(c - O^*) \tag{10}$$

where c represents the number of C atoms.

2.5. Other analysis

The concentrations of primary organic carbon (POC) and secondary organic carbon (SOC) were estimated based on the EC-tracer method, which has been widely used in previous studies (Lin et al., 2009; Zhou et al., 2023) as follows,

$$SOC = OC - EC \times (OC/EC)_{min} \tag{11}$$

$$POC = OC - SOC \tag{12}$$

where $(OC/EC)_{min}$ denotes the minimum OC/EC ratio during the sampling period at each site (Castro et al., 1999).

In addition, the potential source contribution function (PSCF) analysis based on the HYSPLIT model was performed to identify the source areas of atmospheric WSOC following the method described by Li et al. (2023). And here, the median of WSOC concentrations during the sampling period was used as the threshold criteria. Besides, a *t*-test (two sample equal variance) with two-tails at the 95 % confidence level was executed to evaluate the significance level of data differences in this study.

3. Results and discussion

3.1. Spatial variations of chemical and optical characteristics of WSOC among different coastal cities

3.1.1. Concentration levels

The mass concentrations of carbonaceous components (e.g., OC, EC and WSOC) during the sampling periods were summarized and shown in Table 1 and Fig. 2. Generally, the concentrations of carbonaceous components exhibited similar spatial variations among the three sites. The highest OC and WSOC average concentrations were observed in TJ (OC: 10.02 ± 6.06 μg·m^{-3}; WSOC: 5.96 ± 3.21 μg·m^{-3}), followed by QD (OC: 8.69 ± 5.60 μg·m^{-3}; WSOC: 4.68 ± 3.01 μg·m^{-3}) and SH (OC: 3.31 ± 1.48 μg·m^{-3}; WSOC: 2.01 ± 0.85 μg·m^{-3}). The higher concentrations in northern cities ($p < 0.01$) might be related to the increased anthropogenic emissions during the wintertime heating period in northern China (Rai et al., 2021). The WSOC concentrations observed in this study were lower than those previously reported in other Chinese inland cities, such as Beijing (Du et al., 2014a; Li et al., 2020b), Xi'an (Li et al., 2020a; Shen et al., 2017; Yuan et al., 2020), Ji'nan (Wen et al., 2021) and Nanjing (Bao et al., 2022; Xie et al., 2020). The PSCF maps of WSOC showed that WSOC in TJ and QD was mainly affected by the transport of aerosols from the southern edge of the North China Plain, which was one of the most polluted regions in China (Zhang et al., 2021) and the impacts of long-range transmission from the northwest direction cannot be ignored (Fig. S3). In contrast, WSOC in SH was generally impacted by the emissions from local and its surrounding regions such as Jiangsu and Zhejiang provinces.

The average WSOC/OC ratio (0.55–0.61 on average, Table 1) measured at the three sites was a little higher than the values reported in other studies (0.29–0.50 on average) (Choudhary et al., 2021; Li et al., 2020a; Liu et al., 2019; Yuan et al., 2020). The higher WSOC/OC ratio might be associated with the secondary formation and/or sources with a high WSOC/OC emission ratio such as biomass burning (Jin et al., 2020; Salma et al., 2010; Zhang et al., 2022). During the study period, the OC/EC ratio varied from 4.38 to 15.33 with a mean value of 7.99 ± 2.08, 6.45 ± 1.15, 10.05 ± 2.69 in TJ, QD and SH, respectively. The OC/EC ratio was overall higher than 2.0 and fell within the range of 4.8–21.6 reported for biomass burning aerosols in previous studies (Srinivas et al., 2016; Tang et al., 2020). This further suggested the important impacts of biomass burning and secondary formation on the carbonaceous components in the three cities.

3.1.2. Light absorption and fluorescence properties

Abs_{365} and MAE_{365} were commonly used to evaluate the light absorption ability of WS-BrC. Fig. 2 and Table 1 demonstrated the average Abs_{365} and MAE_{365} values in the three cities. MAE_{365} varied from 0.47 to 1.34 m^2·g^{-1} (mean value: 0.89 ± 0.22 m^2·g^{-1}) in TJ, from 0.12 to 1.74 m^2·g^{-1} (mean value: 1.03 ± 0.34 m^2·g^{-1}) in QD and from 0.35 to 0.81 m^2·g^{-1} (mean value: 0.56 ± 0.11 m^2·g^{-1}) in SH. Overall, the MAE_{365} values were comparable to or a little higher than those reported in Guangzhou of China, Leipzig/Melpitz of Germany and Los Angeles of the United States (0.70–0.86 m^2·g^{-1}) (Fan et al., 2016; Liu et al., 2018; Soleimanian et al., 2020; Teich et al., 2017). However, they were much lower than those reported in heavily polluted cities, such as Beijing, Xi'an and Nanjing in China (1.04–1.85 m^2·g^{-1}) and New Delhi, Patiala and Kanpur in India (1.16–1.60 m^2·g^{-1}) (Chen et al., 2018; Cheng et al., 2016; Huang et al., 2018; Kirillova et al., 2014b; Satish et al., 2017; Srinivas et al., 2016; Yan et al., 2015; Yuan et al., 2020). Compared among the three coastal cities, MAE_{365} values ranked from high to low as QD > TJ > SH ($p < 0.05$). The varieties in light absorption ability could be attributed to the different sources and formation mechanisms of WS-BrC in different regions. For example, coal combustion or biomass burning

Table 1
Statistical summary of mass concentrations of carbonaceous components in $PM_{2.5}$, and light-absorbing and fluorescent parameters of WSOC in the three cities.

Species	Tianjin	Qingdao	Shanghai
	Range (average ± std.)	Range (average ± std.)	Range (average ± std.)
OC ($\mu g \cdot m^{-3}$)	1.93–32.18 (10.02 ± 6.06)	1.63–31.64 (8.69 ± 5.60)	1.69–7.98 (3.31 ± 1.48)
EC ($\mu g \cdot m^{-3}$)	0.35–2.53 (1.20 ± 0.53)	0.31–4.23 (1.34 ± 0.83)	0.18–0.73 (0.35 ± 0.16)
WSOC ($\mu g \cdot m^{-3}$)	1.67–14.07 (5.96 ± 3.21)	1.13–17.19 (4.68 ± 3.01)	0.97–4.59 (2.01 ± 0.85)
POC ($\mu g \cdot m^{-3}$)	1.66–11.86 (5.64 ± 2.47)	1.37–18.52 (5.86 ± 3.62)	0.91–3.64 (1.72 ± 0.79)
SOC ($\mu g \cdot m^{-3}$)	0.00–20.32 (4.38 ± 3.94)	0.00–13.12 (2.83 ± 2.49)	0.00–4.34 (1.59 ± 0.94)
OC/EC	4.69–13.27 (7.99 ± 2.08)	4.38–9.02 (6.45 ± 1.15)	4.96–15.33 (10.05 ± 2.69)
WSOC/OC	0.37–0.87 (0.60 ± 0.12)	0.23–0.81 (0.55 ± 0.12)	0.49–0.76 (0.61 ± 0.07)
Abs_{365} (Mm^{-1})	0.89–18.71 (5.57 ± 3.83)	0.21–16.02 (4.80 ± 3.09)	0.33–2.40 (1.12 ± 0.53)
MAE_{365} ($m^2 \cdot g^{-1}$)	0.47–1.34 (0.89 ± 0.22)	0.12–1.74 (1.03 ± 0.34)	0.35–0.81 (0.56 ± 0.11)
$AAE_{330-400}$	3.67–7.34 (6.54 ± 0.64)	4.70–12.58 (9.17 ± 0.88)	5.46–9.13 (6.61 ± 0.68)
FI	1.36–1.66 (1.48 ± 0.06)	1.34–1.75 (1.58 ± 0.09)	1.42–1.82 (1.57 ± 0.09)
BIX	0.84–1.10 (0.97 ± 0.06)	0.74–1.26 (1.08 ± 0.11)	0.91–1.25 (1.02 ± 0.08)
HIX	2.09–3.52 (2.91 ± 0.37)	1.23–2.38 (1.69 ± 0.32)	1.42–2.61 (1.98 ± 0.26)

related heating activities were more extensive during wintertime in TJ and QD in northern China, which might cause increased emissions of much stronger light-absorbing organic species (Yan et al., 2017). Especially, the QD site was located in suburban areas and surrounded by villages with significant residential combustion activities in winter. Fig. S4a depicted that the light absorption coefficients of WSOC were strongly correlated with EC concentrations in the three cities (TJ: $r = 0.87$, QD: $r = 0.90$, SH: $r = 0.79$; $p < 0.01$), indicating that WS-BrC was closely correlated with combustion sources, as EC was usually described as a tracer for primary combustion emissions (Cabada et al., 2004). Moreover, Abs_{365} also exhibited strong correlations with SOC ($r = 0.96$, 0.88, 0.76 in TJ, QD and SH, respectively, $p < 0.01$; see Fig. S4b), suggesting that secondary formation was another important contributor to light absorption species apart from primary emissions, especially for TJ.

Fluorescent components in WSOC were resolved by EEM-PARAFAC analysis and the corresponding spectra were shown in Fig. 3. Generally, five fluorophores were resolved in TJ (C1-C5), and four fluorophores were identified in QD (P1-P4) and SH (F1-F4), respectively. Component C1 (Ex/Em = 250 (325)/394 nm), C2 (Ex/Em = 250 (305/350)/426 nm), C4 (Ex/Em = 250/418 nm), and C5 (Ex/Em = 260 (375)/497 nm) in TJ and P1 (Ex/Em = 250 (320)/397 nm), P2 (Ex/Em = 250 (360)/462 nm), P4 (Ex/Em = 250/389 nm) in QD, as well as F1 (Ex/Em ≤ 250 (320)/394 nm), F2 (Ex/Em = 250 (295/350)/458 nm), F4 (Ex/Em = 265/294 (394) nm) in SH were identified as humic-like substances (HULIS). Among them, C1, C4, P1, P4, F1 and F4 could be further classified as less-oxygenated species (LO-HULIS), while C2, C5, P2 and F2 were corresponding to highly-oxygenated species (HO-HULIS) (Chen et al., 2020; Chen et al., 2016b). The LO-HULIS was usually associated with anthropogenic emissions or continental sources (Wen et al., 2021), while HO-HULIS might be potentially influenced by biomass burning or secondary formation processes. The second peak at high Ex wavelength (Ex ≥350 nm) of these HO-HULIS (i.e., C2, C5, P2 and F2) suggested there might contain condensed aromatic moieties and conjugated bonds. Meanwhile, the longer Em wavelength might be associated with higher aromaticity and unsaturated chemical structures from biomass burning or secondary formation (Deng et al., 2022; Jiang et al., 2022b). Apart from HULIS, protein-like substances (PRLIS) with Ex and Em distributed in shorter wavelength areas (Ex/Em = 200–300/275–360 nm) were also

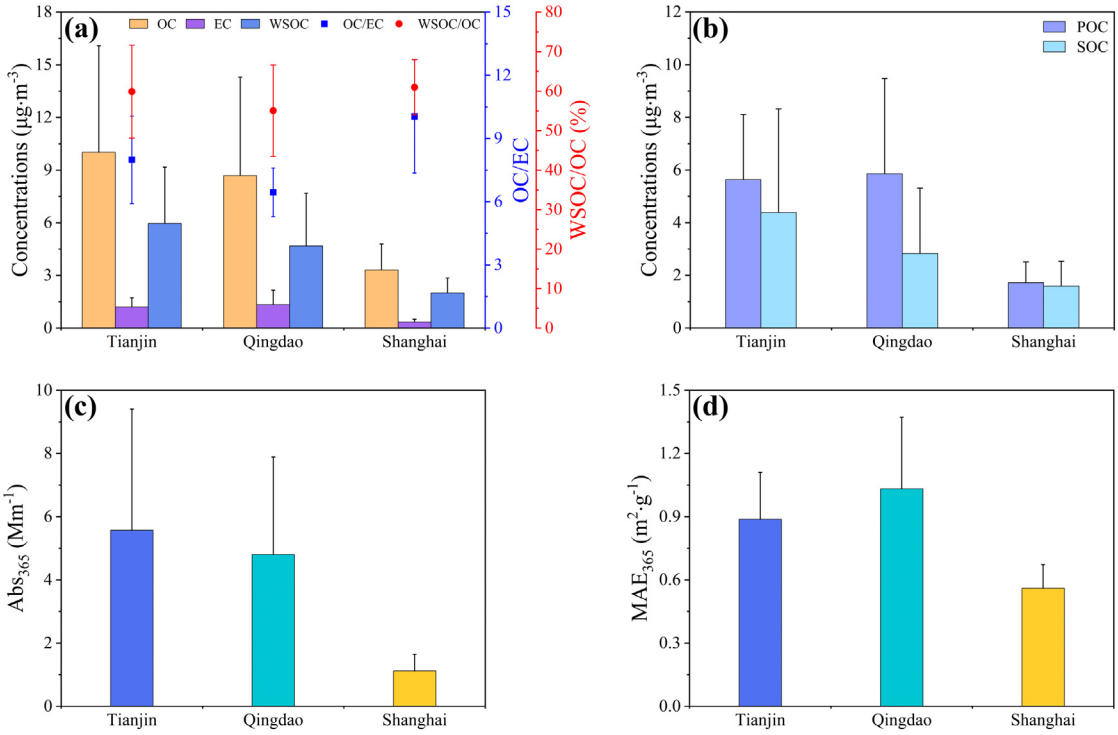

Fig. 2. (a) The average mass concentrations of OC, EC, WSOC and the ratios of OC/EC and WSOC/OC, (b) the mass concentrations of POC and SOC, (c) Abs_{365}, and (d) MAE_{365} of WSOC at the three sampling sites.

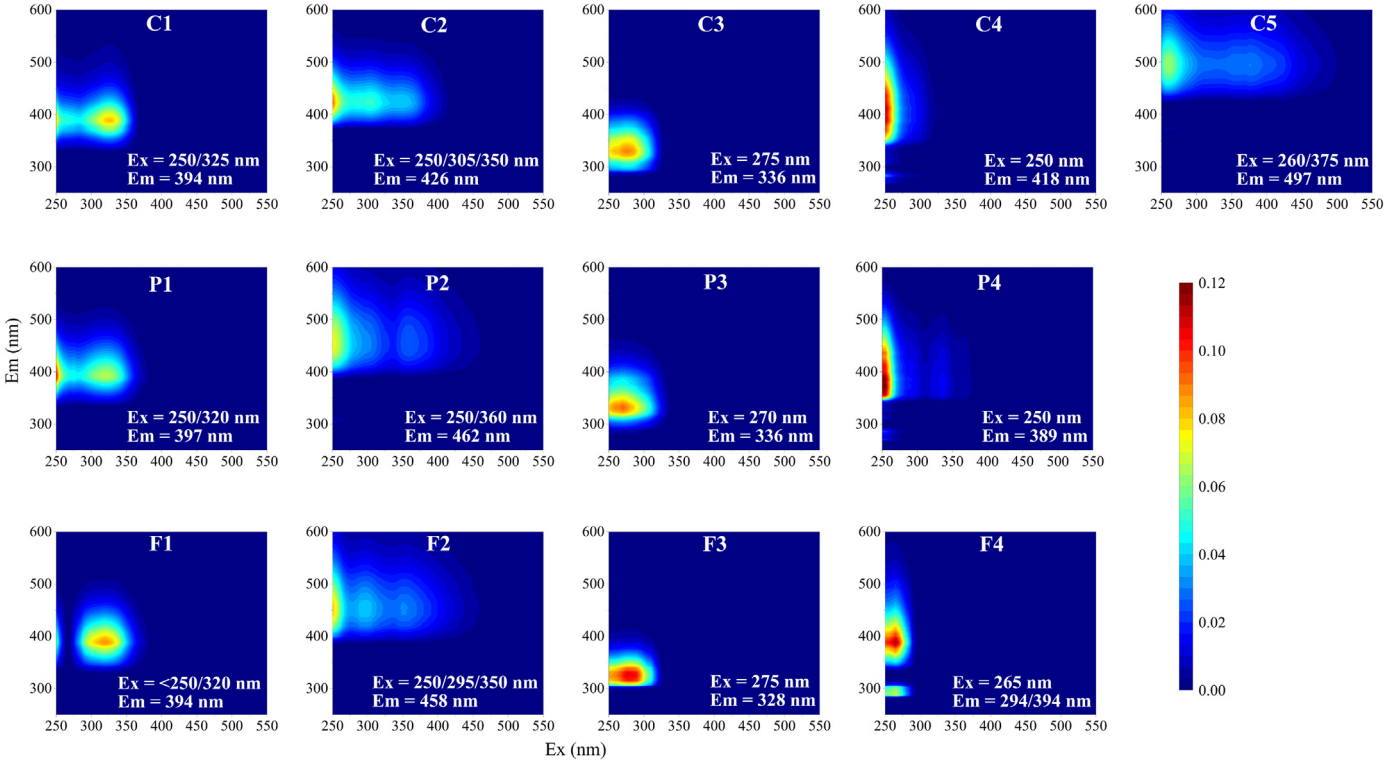

Fig. 3. The fluorescent components in WSOC identified by the EEM-PARAFAC analysis in (C1-C5) Tianjin, (P1-P4) Qingdao, and (F1-F4) Shanghai.

identified (Chen et al., 2016b). In this study, C3 (Ex/Em = 275/336 nm), P3 (Ex/Em = 270/336 nm) and F3 (Ex/Em = 275/328 nm) components were related to PRLIS (Chen et al., 2016a; Chen et al., 2020). Previous studies indicated that the spectra of PRLIS in atmospheric particle samples might be highly overlapped with that of naphthalene and had a strong correlation with fossil fuel combustion derived low molecular weight n-alkanes (Deng et al., 2022; Wu et al., 2019). Overall, LO-HULIS accounted for the highest proportion (52–60 %) in the fluorescent chromophores of WSOC at the three sites, followed by HO-HULIS (15–31 %) and PRLIS (17–31 %) (Fig. S5).

The fluorescence indices of WSOC were further investigated and summarized in Table 1. The HIX was used to evaluate the aromaticity of organic matters, and a higher HIX value usually corresponds to a higher degree of polycondensation and aromaticity (Qin et al., 2018). The HIX values in TJ (2.91 ± 0.37), QD (1.69 ± 0.32) and SH (1.98 ± 0.26) in this study were comparable to those of primary emitted aerosols (0.6–3.4) and fresh secondary organic aerosols (SOA, 1.7–2.3) (Deng et al., 2022; Fu et al., 2015; Lee et al., 2013; Tang et al., 2021; Xie et al., 2016), but lower than those of aged SOA (4.2–6.1) (Lee et al., 2013). This suggested the relatively lower aging and humified degree of WSOC, which was consistent with the highest contributions by LO-HULIS in the three cities. Combined with different fluorescence indices, Fig. S6 showed that the indices in this study were mainly distributed in the region close to those for aerosols from primary emissions and fresh secondary formation (Wu et al., 2021). Specifically, the indices of TJ were comparable to those from biomass burning (Fu et al., 2015; Tang et al., 2021), while the indices of QD and SH were close to the values of continental or biological aerosols and fresh SOA (Li et al., 2022).

3.1.3. Molecular composition characterization

The molecular composition of WSOC was determined based on FT-ICR MS analysis in the negative ESI mode. The number of the identified formulas and intensity-weighted molecular parameters were summarized in Table S1. Generally, a larger number of compounds were identified in QD (5877 ± 984) than those in TJ (5495 ± 168) and SH (5687 ± 98), indicating the WSOC compositions in QD might be more complex. Nonetheless, there were similar proportional contributions by each subgroup of the identified molecular compounds at the three sites. CHON compounds were the predominant subgroup (35–43 % of the total formulas), followed by sulfur-containing compounds (including CHONS and CHOS groups, 24–43 %), CHO compounds (20–26 %) and HCCs (1–7 %) (Fig. S7). Therein, about 83–91 % of the CHON compounds contained oxygen-to-nitrogen ratio (O/N) ≥ 3, indicating such compounds might contain at least one nitro (-NO_2) or nitrooxy (-ONO_2) functional group, which might be nitro-substituted compounds or organonitrates (Song et al., 2019). The excessive number of O atoms indicated that these compounds might also contain other O-containing functional groups such as hydroxyl and carboxylic functional groups (Lin et al., 2012).

About 70–85 % of the CHONS compounds had a ratio of O/(4S + 3 N) ≥ 1, which could account for the existence of both sulfate (-OSO_3H) and nitrate (-ONO_2) functional groups, suggesting that such compounds might be nitrooxy-organosulfates (NOSs) (Jiang et al., 2022a). These compounds might be generated by the oxidation of biogenic/anthropogenic precursors (e.g., VOCs) in the presence of NO_x and SO_2 (Wang et al., 2021a). The Van Krevelen (VK) diagram of CHONS compounds shown in Fig. S8 indicated that the CHONS compounds were mainly concentrated in the region of O/C > 0.5 and H/C > 1.5. Their relative abundance increased with the O/C ratio within a certain range, implying there were more NOSs with a higher degree of oxidation, and atmospheric oxidation might be an important factor affecting the formation of NOSs (Wang et al., 2021b).

Most CHOS compounds had the oxygen-to-sulfur ratio (O/S) > 4, indicating that such compounds might contain one sulfate (-OSO_3H) or sulfonate (-SO_3) functional groups, which might be organosulfates formed by the oxidation of VOCs in the presence of highly acidic sulfate seed aerosols (Riva et al., 2015). Notably, several formulas previously identified in biomass burning (e.g., $C_9H_{12}O_4$, $C_9H_{10}O_4$, $C_{12}H_{14}O_5$, $C_{15}H_{19}O_8N$, $C_{19}H_{26}O_7N_2$, etc.), coal combustion emissions (e.g., $C_8H_6O_4$, $C_{12}H_{16}O_4$, $C_7H_7O_4N$, $C_{12}H_{10}O_8N_2$, $C_9H_7O_5NS$, $C_{10}H_7O_7NS$, $C_8H_{10}O_5S$, $C_9H_{12}O_6S$, etc.) and SOA generated by oxidation of VOCs (e.g., $C_5H_7O_4N$, $C_{10}H_{17}O_7NS$, $C_{10}H_{17}O_9NS$, $C_{15}H_{24}O_7S$, $C_9H_{16}O_6S$, $C_{10}H_{18}O_6S$, $C_{12}H_{24}O_5S$, etc.) were detected in all samples analyzed in this study (Ng et al., 2008; Perraud et al., 2010; Song et al.,

2019, 2018; Surratt et al., 2008; Tang et al., 2020; Wang et al., 2021a), implying that there were non-ignorable impacts of both primary emissions and secondary formation on the molecular composition of WSOC at the three sites. Besides, several CHOS compounds (e.g., $C_{16}H_{26}O_3S$, $C_{17}H_{28}O_3S$, $C_{18}H_{30}O_3S$, $C_{19}H_{32}O_3S$), which had been reported to be emitted from cargo ships with heavy fuel oils in port cities, were also detected in all samples in this study (Bai et al., 2020). Such CHOS compounds accounted for a non-negligible proportion of CHOS compounds at the three sampling sites (TJ: 0.3–1.9 %; QD: 0.2–1.3 %; SH: 0.7–4.0 %; the ratio of relative abundance). This suggested that cargo ship emissions might have non-negligible effects on the molecular composition of aerosols in the three port cities.

Discrepancies in the molecular composition also existed among the three sites. The formulas identified in TJ and QD had similar DBE_w, DBE/C_w and $AI_{mod,w}$, and all were higher than those in SH (DBE/C_w: $p < 0.05$; DBE_w and $AI_{mod,w}$: $p > 0.05$), indicating that the molecule of WSOC in TJ and QD had a higher degree of unsaturation and aromaticity. The unique formulas identified at each site relative to the other two sites were displayed in the VK plots (Fig. 4). Molecules in different regions in the VK diagram were further divided into eight compound categories (A-H) according to the O/C and H/C ratios. From this, the unique formulas in TJ were mainly carboxylic-rich alicyclic molecules (CRAMs-like) with lower H/C and O/C values. The unique formulas in QD included CRAMs-like molecules, highly oxygenated organic compounds and carbohydrates-like substances with higher oxidation degree (higher O/C ratio). In contrast, more aliphatic/peptides-like species or CRAMs-like molecules with higher saturation and lower oxidation degree (in the upper left region of the VK diagram) could be found in SH. These discrepancies might be related to the differences in sources or atmospheric chemical processes in different regions.

3.2. Influences of continental versus marine air masses on the light absorption properties and molecular composition

3.2.1. Impacts on the light absorption properties

Air masses arriving at the three sampling sites were calculated and divided into continental and marine air masses. The average Abs_{365} of WSOC affected by the continental air masses observed at the three sites (TJ: 5.71 ± 3.92 Mm^{-1}; QD: 5.06 ± 3.12 Mm^{-1}; SH: 1.23 ± 0.32 Mm^{-1}) were slightly higher ($p > 0.05$) than those affected by the marine air masses (TJ: 4.64 ± 3.06 Mm^{-1}; QD: 4.07 ± 2.86 Mm^{-1}; SH: 1.06 ± 0.60 Mm^{-1}) (Fig. S9). This agreed well with a recent study by Mo et al. (2022), which also found that Con-influenced WSOC exhibited higher light absorption coefficient. To be noted that, a larger sample size is needed to draw more reliable conclusions. Several key BrC chromophores (e.g., $C_6H_5O_3N$, $C_8H_9O_3N$, $C_{10}H_{17}O_7NS$, $C_{16}H_{26}O_3S$, $C_{17}H_{28}O_3S$, $C_{18}H_{30}O_3S$, $C_{19}H_{32}O_3S$) identified in a previous study (Bai et al., 2020) were also detected in this study. Cleary, all of these chromophores had a higher proportion in Con-influenced WSOC (TJ: 2.9 %; QD: 2.1 %; SH: 5.0 % in total, the ratio of relative abundance and the same below) than those in Mar-influenced WSOC (TJ: 2.7 %; QD: 1.2 %; SH: 2.9 % in total; $p > 0.05$). However, the MAE_{365} values of Con-influenced WSOC were equivalent to or only slightly higher than those affected by marine air masses, which might be because of the corresponding much higher WSOC mass concentrations under the influence of continental air masses (Fig. S9). Furthermore, it might also be attributed to the weaker light-absorbing components in the marine source aerosols.

3.2.2. Diversities of molecular composition under the influence of different air masses

The molecular characterization of WSOC in samples affected by continental and marine air masses was further investigated based on the results of FT-ICR MS analysis. As shown in Table S1, there were more formulas identified in the Con-influenced samples (from 5663 to 6861) than that in the Mar-influenced samples (from 4893 to 5589; $p > 0.05$). And compounds in the Con-influenced samples had higher average molecular weight at all sites, indicating Con-influenced samples might have more complex molecular composition. The higher $AI_{mod,w}$ and DBE_w values of Con-influenced samples in TJ and QD further suggested these samples were characterized with higher aromaticity and unsaturation than Mar-influenced samples. In contrast, Con-influenced samples in SH were less aromatized and unsaturated compared to Mar-influenced samples, which might be related to the aging of Mar-influenced organic aerosols emitted from the open ocean during long-distance transmission, while the continental air masses transmitted to SH were mainly from near regions (Fig. S2). Accordingly, molecules of Con-influenced WSOC generally had a higher degree of aromaticity and unsaturation, but the possible aging process during the transmission of air masses should also be considered.

CHON compounds were the most abundant compounds in all samples. These compounds were classified into different subgroups according to N and O numbers, and here we only discussed the N_1O_x subgroup with the highest proportion. As shown in Fig. 5a, the N_1O_3-N_1O_{13} subgroups dominated the total CHON compounds, with the number of subgroups increasing from N_1O_1 to N_1O_8, and then decreasing from N_1O_9 to N_1O_{15} under different cases. However, the distributions of the formulas of N_1O_x subgroups varied at different sampling sites under the influences of marine and continental air masses. For example, all of the N_1O_x subgroups exhibited a larger number of formulas in Mar-influenced samples than those in Con-influenced samples in SH, indicating that there might be more oxygen-containing functional groups in Mar-influenced samples in SH.

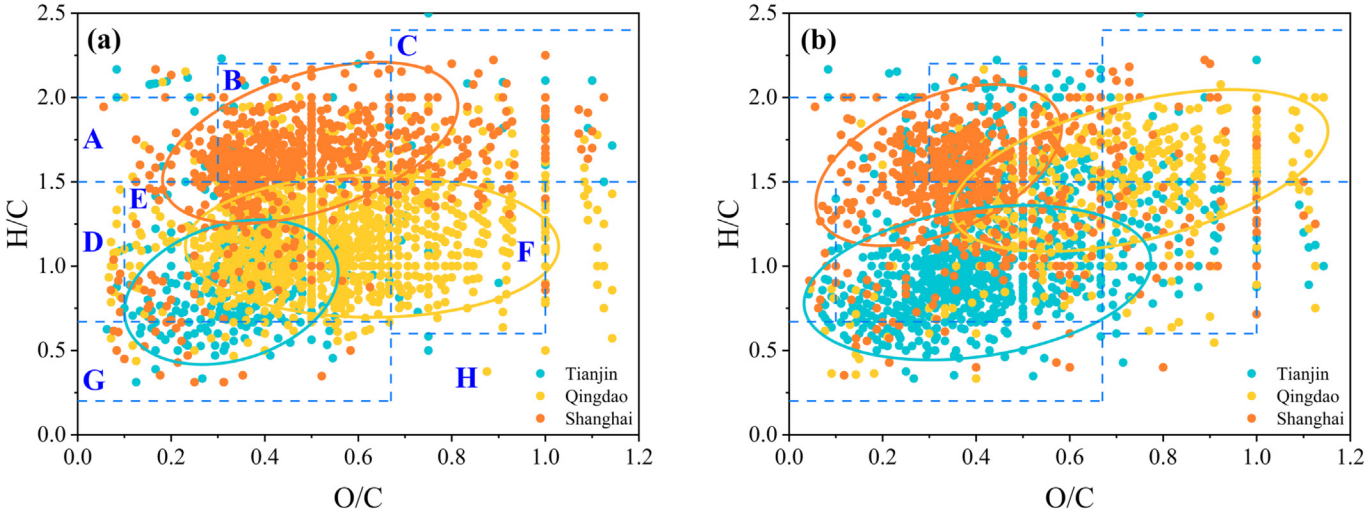

Fig. 4. The Van Krevelen diagrams of unique formulas of each site relative to the other two sites in samples affected by (a) continental and (b) marine air masses.

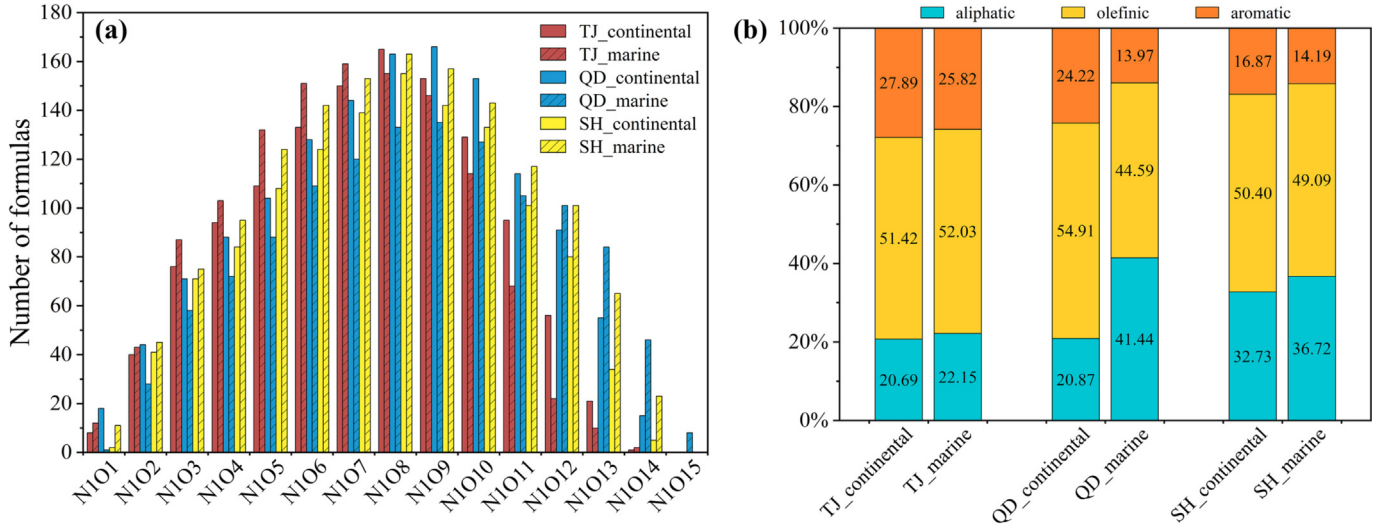

Fig. 5. (a) Distributions of the $CHON_1$ compounds according to the number of N and O atoms, and (b) relative percentages of the molecular formulas for aliphatic ($AI_{mod} = 0$), olefinic ($0 < AI_{mod} < 0.5$), and aromatic ($AI_{mod} \geq 0.5$) subgroups in CHON compounds at the three sampling sites.

This might be associated with the transmission aging process. By contrast, the formulas number of N_1O_1-N_1O_7 subgroups in Mar-influenced samples was relatively larger in TJ, while N_1O_8-N_1O_{13} subgroups were relatively more abundant in Con-influenced samples, suggesting there might be less highly-oxygenated nitrogen-containing compounds in Mar-influenced samples in TJ. On the contrary, Mar-influenced samples in QD had more highly-oxygenated species (N_1O_{12}-N_1O_{15}). Fig. 5b interpreted that Mar-influenced samples were characterized with a lower proportion of aromatic CHON compounds (14–26 % in formulas), whereas, they were enriched with more aliphatic compounds (22–41 % in formulas), which might be associated with the emission of primary marine biological components (Mo et al., 2022). Furthermore, the H/C_w ratios ($AI_{mod,w}$ values) for the CHON compounds in Mar-influenced samples were within the range of 1.07–1.28 (0.23–0.42), which were slightly higher (lower) than those found for CHON compounds in Con-influenced samples (H/C_w: 1.06–1.20; $AI_{mod,w}$: 0.31–0.42), respectively. These suggested that the CHON compounds in Mar-influenced samples might be with higher degree of saturation but low aromaticity, which might be related to biogenic marine emissions.

In this study, more S-containing (CHONS and CHOS) compounds were identified in Con-influenced samples. This might be associated with the reaction of high concentrations of biogenic/anthropogenic precursors (e.g., isoprene, monoterpenes, polycyclic aromatic hydrocarbons) and anthropogenic pollutants (NO_x, SO_2, sulfate) (Brüggemann et al., 2020; Wang et al., 2020). CHONS compounds in Con-influenced samples had lower O/C_w but higher DBE_w and DBE/C_w values, indicating these compounds had a lower degree of oxidation and saturation but higher aromaticity (Table S1). As shown in Fig. S10, most of the unique CHONS compounds in Con-influenced samples were characterized with 5–25 C atoms, 2–15 O atoms and 1–11 of DBE values, which had a wider range than those in Mar-influenced samples. The unique CHONS compounds with higher abundance mainly included $C_5H_5O_4NS$, $C_5H_6O_4N_2S$, $C_{10}H_7O_8NS$, $C_{11}H_7O_9NS$, $C_{13}H_{26}O_{10}N_2S$, $C_{16}H_{22}O_{11}N_2S$, etc. These compounds with two N atoms might contain a nitrogen-containing heterocyclic structure. However, there was no more specific structure information determined in this study and further research was needed to reveal their structures. Additionally, CHOS compounds could be further classified into $CHOS_1$ and $CHOS_2$ subgroups, with $CHOS_1$ compounds accounting for the majority of CHOS compounds (96–99 % in formulas). According to the O*/C ratio and AI* values, six subgroups (A-F) of $CHOS_1$ compounds were further classified and plotted in Fig. 6. Obviously, there were a larger number of high unsaturated and unsaturated aliphatic CHOS compounds with higher O/S ratio ($O/S \geq 10$, subgroup C and D) in Con-influenced samples (55–176 formulas with a proportion of 6.1–15.6 % in CHOS formulas) than those in Mar-influenced samples (15–93 formulas with a proportion of 2.0–15.5 % in CHOS formulas). These high-O/S ratio compounds might be related to SOA from biomass burning or the oxidation of biogenic VOCs (Su et al., 2022).

3.3. Halogen-containing organic compounds

To be noted that, a portion of molecules were identified as organohalogen compounds at the three sampling sites in this study. The number of formulas and molecular parameters of these HCCs were summarized in Table S1. Generally, the formulas and relative number contributions of HCCs in all identified formulas in Con-influenced samples (TJ: 207 and 3.66 %; QD: 92 and 1.34 %; SH: 336 and 5.81 %) were lower than those in Mar-influenced samples (TJ: 373 and 7.00 %; QD: 308 and 6.29 %; SH: 373 and 6.67 %) (Figs. 7 and S7). Furthermore, CHOX (53–174 formulas and 0.77–3.26 % proportion) and CHONX (21–198 formulas and 0.30–3.54 % proportion) were the most abundant subgroups of HCCs in all samples, especially CHOCl (32–158 formulas and 0.46–2.83 % proportion) and CHONCl (15–198 formulas and 0.22–3.54 % proportion) compounds. Previous studies indicated that the oxidation of VOCs by the Cl atom was an important source of organic aerosols in marine boundary layers and coastal regions (Cai and Griffin, 2006). And the oxidation of organics in marine areas by the Cl atom might be analogous to or even exceed that of OH under some conditions (Cabanas et al., 2005; Spicer et al., 1998). In marine areas, water was volatilized from seawater droplets under the actions of the wave by leaving behind dissolved solid suspended particles mainly containing sodium chloride (NaCl). Therefore, NaCl might have reacted with gaseous substances such as N_2O_5 or $ClONO_2$ to generate Cl atoms (Finlaysonpitts, 1993; Graedel and Keene, 1995). Besides, the high content of Cl atoms in marine or coastal areas could also be attributed to the photolysis of chlorine-containing molecules (Chang et al., 2002; Singh and Kasting, 1988; Spicer et al., 1998).

The CHOCl and CHONCl compounds in Mar-influenced samples had a higher degree of saturation, but lower aromaticity compared to those in Con-influenced samples (see Table S1). This might be because the precursors from marine were generally saturated compounds such as monoterpenes (Yu and Li, 2021). As shown in Fig. S11, a portion of the CHOCl and CHONCl compounds contained more than six C atoms and $DBE \geq 4$, suggesting there might be a benzene ring structure and the Cl atom might exist by replacing the H atom on the alkyl group connecting with the benzene ring. Some compounds with lower unsaturation ($DBE \leq 3$) might be the reaction products of the Cl atom and some heterocyclic aromatic

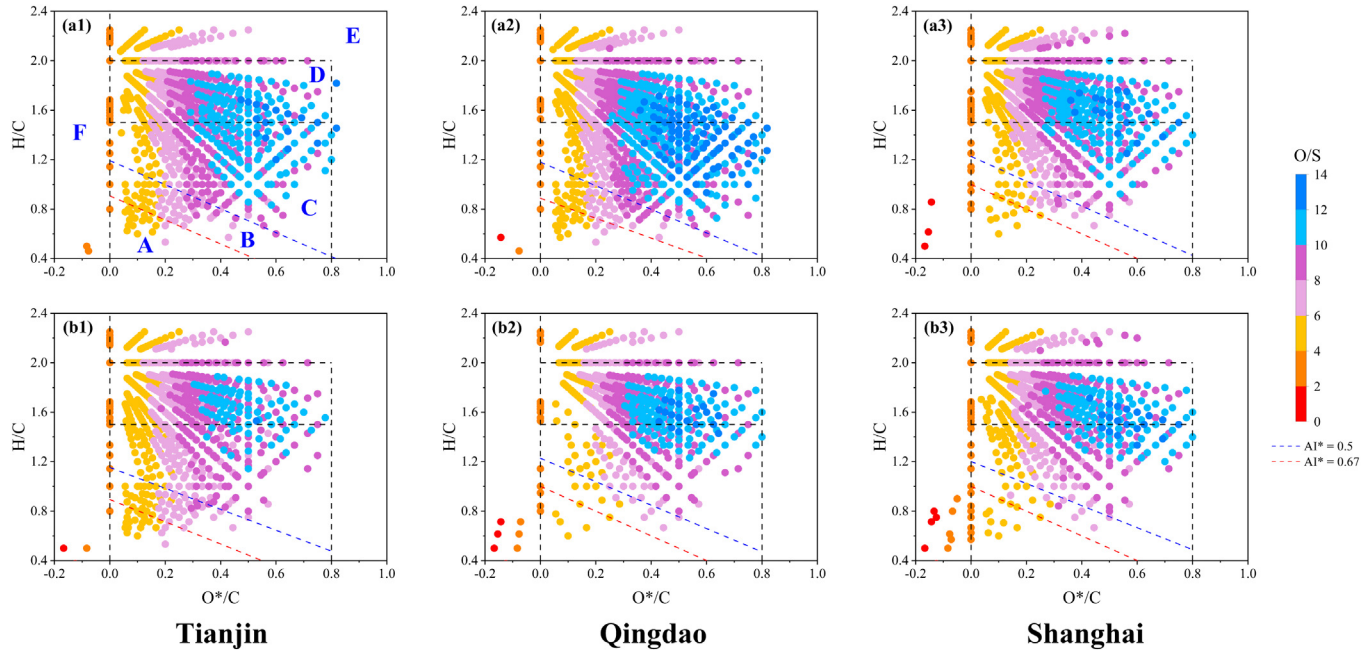

Fig. 6. Modified Van Krevelen diagrams of $CHOS_1$ in samples affected by (a1-a3) continental air masses and (b1-b3) marine air masses at each site.

hydrocarbons or monoterpenes (e.g., furan and its derivatives, α-pinene, etc.) (Cabanas et al., 2005; Cai and Griffin, 2006). In general, these organochloride compounds might be formed by the reaction of Cl atoms with biologic or anthropogenic VOCs through the substitution of H atoms in C—H bonds or the addition of C═C bonds (Ziemann and Atkinson, 2012).

Furthermore, certain Br/I-containing compounds were also identified in this study, which might be the oxidation products of VOCs by anthropogenic or oceanic Br/I atoms. Previous studies had indicated that Br could induce significant multiphase chemistry in organic aerosols in the marine boundary layer (Lambe et al., 2022; Liao et al., 2012). Meanwhile, organic compounds from the reaction of iodine or iodinated methane from coastal biota or biologically active sea surfaces with VOCs could be important components in iodine-initiated new particle formation in coastal regions (Wan et al., 2022). Therefore, the reaction of halogen atoms and VOCs emitted from the ocean might be an important source of HCCs in Mar-influenced samples. More future research should be proceeded to reveal the formation mechanism and composition of HCCs.

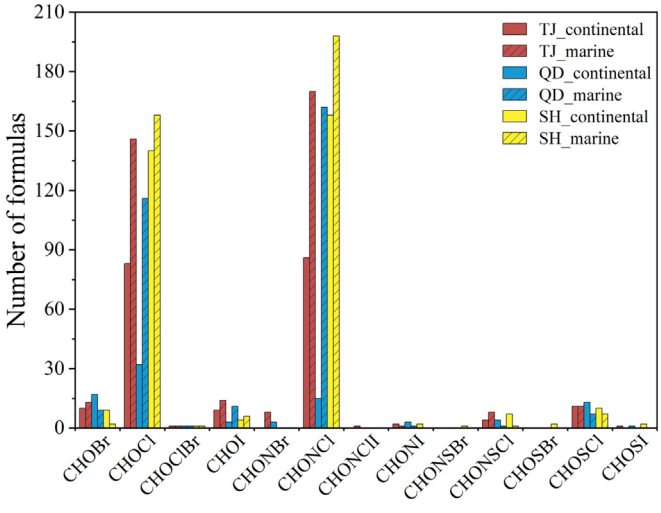

Fig. 7. Distributions of the subgroups of HCCs according to the C, H, O, N, S atoms and different types of halogen atom.

4. Conclusions

This study investigated the optical properties and molecular characteristics of WSOC in three coastal cities in eastern China. The results suggested that the mass concentrations of carbonaceous components and light absorption coefficients of WSOC ranked from high to low from north to south as TJ > QD > SH, which might be related to the increased anthropogenic emissions during the winter heating period in northern cities. Moreover, the EEM-PARAFAC analysis indicated that fluorescent components of WSOC mainly included two types, that is, HULIS and PRLIS. Less-oxygenated HULIS (52–60 %) was the most abundant fluorophore, which might be associated with the anthropogenic emissions or continental sources, followed by highly-oxygenated HULIS (15–31 %, which might be mainly from secondary formation), and PRLIS (17–31 %). The fluorescence indices further demonstrated that the fluorescent components in WSOC were mainly from primary emissions, while secondary formation was also non-negligible.

Molecular characteristics of WSOC were analyzed by (ESI-) FT-ICR MS and the identified formulas were classified into five main subgroups, including CHO, CHON, CHONS, CHOS and HCCs. The CHON compounds were the predominant subgroup in all samples, accounting for 35–43 % of the identified compounds, followed by sulfur-containing compounds (including CHONS and CHOS groups, 24–43 %), CHO compounds (20–26 %) and HCCs (1–7 %). Many compounds identified in this study had been proven to emit from biomass burning and coal combustion or secondary formation in previous studies, indicating that there were important impacts of both primary emissions and secondary formation on the molecular composition of WSOC at the three sites. Moreover, many CHOS compounds (e.g., $C_{16}H_{26}O_3S$, $C_{17}H_{28}O_3S$, $C_{18}H_{30}O_3S$, and $C_{19}H_{32}O_3S$) emitted from cargo ships were identified in all analyzed samples, indicating the non-negligible contribution of port emissions to the composition of WSOC at the three coastal sites. In addition, there existed discrepancies in molecular characteristics of WSOC between different cities, which may be related to the differences of sources or atmospheric chemical processes in different regions and needs more in-depth research.

Samples affected by continental and marine air masses were further compared. The average Abs_{365} of Con-influenced WSOC was higher than that of Mar-influenced WSOC. By comparison, Mar-influenced samples contained more aliphatic CHON compounds with lower aromaticity, which might be associated with sea-biological activities. In contrast, there were more unsaturated molecules with higher aromaticity in Con-

influenced samples, including CHON and CHONS compounds. In addition, there were a larger number of high unsaturated and unsaturated aliphatic CHOS compounds with a higher O/S ratio (O/S ≥ 10) in Con-influenced samples, which might be related to SOA from biomass burning or the oxidation of biogenic VOCs. To be noted that, HCCs were also discussed in this study. CHOCl and CHONCl compounds were the main HCCs in all samples, and both of them were more abundant in Mar-influenced samples. The HCCs in Mar-influenced samples might be associated with the oxidation of VOCs by halogen atoms. More efforts should be made to better understand the formation mechanism of HCCs compounds in coastal areas in the future. Furthermore, in-depth research on the relationships between molecular composition and light-absorbing properties as well as the formation mechanism of light-absorbing compounds under the influences of different air masses are warranted with a large sample size in different seasons and a long-term field observation in coastal areas.

CRediT authorship contribution statement

Haibiao Chen: Methodology, Data curation, Formal analysis, Investigation, Writing – original draft. **Caiqing Yan**: Conceptualization, Methodology, Resources, Data curation, Writing – review & editing, Visualization, Supervision, Funding acquisition, Project administration. **Qinglong Fu**: Methodology, Investigation, Resources. **Xinfeng Wang**: Review & editing. **Jiao Tang**: Methodology, Investigation, Resources. **Bin Jiang**: Data curation, Investigation, Resources. **Honglei Sun**: Investigation. **Tiancheng Luan**: Investigation. **Qiaoyun Yang**: Investigation, Resources. **Qianbiao Zhao**: Investigation, Resources. **Jun Li**: Resources, Review & editing. **Gan Zhang**: Resources, Review & editing. **Mei Zheng**: Resources, Review & editing. **Xuehua Zhou**: Resources. **Bing Chen**: Resources. **Lin Du**: Resources, Review & editing. **Ruizhi Zhou**: Investigation, Data curation. **Taomeizi Zhou**: Investigation, Data curation. **Likun Xue**: Resources, Review & editing.

Data availability

Data will be made available on request.

Declaration of competing interest

The authors declare that they have no known competing financial interests or personal relationships that could have appeared to influence the work reported in this paper.

Acknowledgment

This study was funded by the National Natural Science Foundation of China (NO. 42205110), Excellent Young Scholar (Overseas) project of Shandong Province (2022HWYQ-049), and State Environmental Protection Key Laboratory of Formation and Prevention of Urban Air Pollution Complex (CX2020080585). Caiqing Yan was specifically supported by Taishan Scholar Project of Shandong Province (NO. tsqn201909018), and Qilu Youth Talent Programme of Shandong University. The authors kindly acknowledge the NOAA Air Resources Laboratory for the provision of the HYSPLIT model.

Appendix A. Supplementary data

Supplementary data to this article can be found online at https://doi.org/10.1016/j.scitotenv.2023.164702.

References

Andreae, M.O., Gelencsér, A., 2006. Black carbon or brown carbon? The nature of light-absorbing carbonaceous aerosols. Atmos. Chem. Phys. 6, 3131–3148. https://doi.org/10.5194/acp-6-3131-2006.

Bai, Z., Zhang, L., Cheng, Y., Zhang, W., Mao, J., Chen, H., et al., 2020. Water/methanol-insoluble brown carbon can dominate aerosol-enhanced light absorption in port cities. Environ. Sci. Technol. 54, 14889–14898. https://doi.org/10.1021/acs.est.0c03844.

Bao, H.Y., Niggemann, J., Luo, L., Dittmar, T., Kao, S.J., 2018. Molecular composition and origin of water-soluble organic matter in marine aerosols in the Pacific off China. Atmos. Environ. 191, 27–35. https://doi.org/10.1016/j.atmosenv.2018.07.059.

Bao, M., Zhang, Y.L., Cao, F., Lin, Y.C., Hong, Y., Fan, M., et al., 2022. Light absorption and source apportionment of water soluble humic-like substances (HULIS) in $PM_{2.5}$ at Nanjing, China. Environ. Res. 206, 112554. https://doi.org/10.1016/j.envres.2021.112554.

Bikkina, S., Kawamura, K., Sarin, M., 2017. Secondary organic aerosol formation over coastal ocean: inferences from atmospheric water-soluble low molecular weight organic compounds. Environ. Sci. Technol. 51, 4347–4357. https://doi.org/10.1021/acs.est.6b05986.

Brüggemann, M., Xu, R., Tilgner, A., Kwong, K.C., Mutzel, A., Poon, H.Y., et al., 2020. Organosulfates in ambient aerosol: state of knowledge and future research directions on formation, abundance, fate, and importance. Environ. Sci. Technol. 54, 3767–3782. https://doi.org/10.1021/acs.est.9b06751.

Cabada, J.C., Pandis, S.N., Subramanian, R., Robinson, A.L., Polidori, A., Turpin, B., 2004. Estimating the secondary organic aerosol contribution to $PM_{2.5}$ using the EC tracer method. Aerosol Sci. Technol. 38, 140–155. https://doi.org/10.1080/02786820390229084.

Cabanas, B., Villanueva, F., Martin, P., Baeza, M.T., Salgado, S., Jimenez, E., 2005. Study of reaction processes of furan and some furan derivatives initiated by Cl atoms. Atmos. Environ. 39, 1935–1944. https://doi.org/10.1016/j.atmosenv.2004.12.013.

Cai, X.Y., Griffin, R.J., 2006. Secondary aerosol formation from the oxidation of biogenic hydrocarbons by chlorine atoms. J. Geophys. Res. - Atmos. 111. https://doi.org/10.1029/2005jd006857.

Castro, L.M., Pio, C.A., Harrison, R.M., Smith, D.J.T., 1999. Carbonaceous aerosol in urban and rural European atmospheres: estimation of secondary organic carbon concentrations. Atmos. Environ. 33, 2771–2781. https://doi.org/10.1016/S1352-2310(98)00331-8.

Chang, S.Y., McDonald-Buller, E., Kimura, Y., Yarwood, G., Neece, J., Russell, M., et al., 2002. Sensitivity of urban ozone formation to chlorine emission estimates. Atmos. Environ. 36, 4991–5003. https://doi.org/10.1016/S1352-2310(02)00573-3.

Chen, Q., Ikemori, F., Mochida, M., 2016a. Light absorption and excitation-emission fluorescence of urban organic aerosol components and their relationship to chemical structure. Environ. Sci. Technol. 50, 10859–10868. https://doi.org/10.1021/acs.est.6b02541.

Chen, Q., Miyazaki, Y., Kawamura, K., Matsumoto, K., Coburn, S., Volkamer, R., et al., 2016b. Characterization of chromophoric water-soluble organic matter in urban, forest, and marine aerosols by HR-ToF-AMS analysis and excitation-emission matrix spectroscopy. Environ. Sci. Technol. 50, 10351–10360. https://doi.org/10.1021/acs.est.6b01643.

Chen, Y.F., Ge, X.L., Chen, H., Xie, X.C., Chen, Y.T., Wang, J.F., et al., 2018. Seasonal light absorption properties of water-soluble brown carbon in atmospheric fine particles in Nanjing, China. Atmos. Environ. 187, 230–240. https://doi.org/10.1016/j.atmosenv.2018.06.002.

Chen, Q., Li, J., Hua, X., Jiang, X., Mu, Z., Wang, M., et al., 2020. Identification of species and sources of atmospheric chromophores by fluorescence excitation-emission matrix with parallel factor analysis. Sci. Total Environ. 718, 137322. https://doi.org/10.1016/j.scitotenv.2020.137322.

Cheng, Y., He, K.B., Du, Z.Y., Engling, G., Liu, J.M., Ma, Y.L., et al., 2016. The characteristics of brown carbon aerosol during winter in Beijing. Atmos. Environ. 127, 355–364. https://doi.org/10.1016/j.atmosenv.2015.12.035.

Choudhary, V., Rajput, P., Gupta, T., 2021. Absorption properties and forcing efficiency of light-absorbing water-soluble organic aerosols: seasonal and spatial variability. Environ. Pollut. 272, 115932. https://doi.org/10.1016/j.envpol.2020.115932.

Deng, J., Ma, H., Wang, X., Zhong, S., Zhang, Z., Zhu, J., et al., 2022. Measurement report: optical properties and sources of water-soluble brown carbon in Tianjin, North China – insights from organic molecular compositions. Atmos. Chem. Phys. 22, 6449–6470. https://doi.org/10.5194/acp-22-6449-2022.

Ding, A., Wang, T., Zhao, M., Wang, T., Li, Z.K., 2004. Simulation of sea-land breezes and a discussion of their implications on the transport of air pollution during a multi-day ozone episode in the Pearl River Delta of China. Atmos. Environ. 38, 6737–6750. https://doi.org/10.1016/j.atmosenv.2004.09.017.

Du, Z.Y., He, K.B., Cheng, Y., Duan, F.K., Ma, Y.L., Liu, J.M., et al., 2014a. A yearlong study of water-soluble organic carbon in Beijing I: sources and its primary vs. secondary nature. Atmos. Environ. 92, 514–521. https://doi.org/10.1016/j.atmosenv.2014.04.060.

Du, Z.Y., He, K.B., Cheng, Y., Duan, F.K., Ma, Y.L., Liu, J.M., et al., 2014b. A yearlong study of water-soluble organic carbon in Beijing II: light absorption properties. Atmos. Environ. 89, 235–241. https://doi.org/10.1016/j.atmosenv.2014.02.022.

Fan, X.J., Wei, S.Y., Zhu, M.B., Song, J.Z., Peng, P.A., 2016. Comprehensive characterization of humic-like substances in smoke $PM_{2.5}$ emitted from the combustion of biomass materials and fossil fuels. Atmos. Chem. Phys. 16, 13321–13340. https://doi.org/10.5194/acp-16-13321-2016.

Fan, Y.B., Liu, C.Q., Li, L.J., Ren, L.J., Ren, H., Zhang, Z.M., et al., 2020. Large contributions of biogenic and anthropogenic sources to fine organic aerosols in Tianjin, North China. Atmos. Chem. Phys. 20, 117–137. https://doi.org/10.5194/acp-20-117-2020.

Finlaysonpitts, B.J., 1993. Chlorine atoms as a potential tropospheric oxidant in the marine boundary-layer. Res. Chem. Intermed. 19, 235–249. https://doi.org/10.1163/156856793x00091.

Fu, P., Kawamura, K., Chen, J., Qin, M., Ren, L., Sun, Y., et al., 2015. Fluorescent water-soluble organic aerosols in the high Arctic atmosphere. Sci. Rep. 5, 9845. https://doi.org/10.1038/srep09845.

Fu, Q.L., Fujii, M., Watanabe, A., Kwon, E., 2022. Formula assignment algorithm for deuterium-labeled ultrahigh-resolution mass spectrometry: implications of the formation mechanism of halogenated disinfection byproducts. Anal. Chem. 94, 1717–1725. https://doi.org/10.1021/acs.analchem.1c04298.

Fuzzi, S., Decesari, S., Facchini, M.C., Matta, E., Mircea, M., Tagliavini, E., 2001. A simplified model of the water soluble organic component of atmospheric aerosols. Geophys. Res. Lett. 28, 4079–4082. https://doi.org/10.1029/2001gl013418.

Gantt, B., Meskhidze, N., Zhang, Y., Xu, J., 2010. The effect of marine isoprene emissions on secondary organic aerosol and ozone formation in the coastal United States. Atmos. Environ. 44, 115–121. https://doi.org/10.1016/j.atmosenv.2009.08.027.

Graedel, T.E., Keene, W.C., 1995. Tropospheric budget of reactive chlorine. Glob. Biogeochem. Cycles 9, 47–77. https://doi.org/10.1029/94gb03103.
He, Q., Tomaz, S., Li, C., Zhu, M., Meidan, D., Riva, M., et al., 2021. Optical properties of secondary organic aerosol produced by nitrate radical oxidation of biogenic volatile organic compounds. Environ. Sci. Technol. 55, 2878–2889. https://doi.org/10.1021/acs.est.0c06838.
Hecobian, A., Zhang, X., Zheng, M., Frank, N., Edgerton, E.S., Weber, R.J., 2010. Water-soluble organic aerosol material and the light-absorption characteristics of aqueous extracts measured over the southeastern United States. Atmos. Chem. Phys. 10, 5965–5977. https://doi.org/10.5194/acp-10-5965-2010.
Huang, R.J., Yang, L., Cao, J., Chen, Y., Chen, Q., Li, Y., et al., 2018. Brown carbon aerosol in urban Xi'an, Northwest China: the composition and light absorption properties. Environ. Sci. Technol. 52, 6825–6833. https://doi.org/10.1021/acs.est.8b02386.
Jiang, H.X., Li, J., Tang, J., Cui, M., Zhao, S.Z., Mo, Y.Z., et al., 2022a. Molecular characteristics, sources, and formation pathways of organosulfur compounds in ambient aerosol in Guangzhou, South China. Atmos. Chem. Phys. 22, 6919–6935. https://doi.org/10.5194/acp-22-6919-2022.
Jiang, H.X., Tang, J., Li, J., Zhao, S.Z., Mo, Y.Z., Tian, C.G., et al., 2022b. Molecular signatures and sources of fluorescent components in atmospheric organic matter in South China. Environ. Sci. Technol. Lett. 9, 913–920. https://doi.org/10.1021/acs.estlett.2c00629.
Jin, Y.L., Yan, C.Q., Sullivan, A.P., Liu, Y., Wang, X.M., Dong, H.B., et al., 2020. Significant contribution of primary sources to water-soluble organic carbon during spring in Beijing, China. Atmosphere 11. https://doi.org/10.3390/atmos11040395.
Kirillova, E.N., Andersson, A., Han, J., Lee, M., Gustafsson, O., 2014a. Sources and light absorption of water-soluble organic carbon aerosols in the outflow from northern China. Atmos. Chem. Phys. 14, 1413–1422. https://doi.org/10.5194/acp-14-1413-2014.
Kirillova, E.N., Andersson, A., Tiwari, S., Srivastava, A.K., Bisht, D.S., Gustafsson, O., 2014b. Water-soluble organic carbon aerosols during a full New Delhi winter: isotope-based source apportionment and optical properties. J. Geophys. Res. - Atmos. 119, 3476–3485. https://doi.org/10.1002/2013jd020041.
Kuang, B.Y., Lin, P., Huang, X.H.H., Yu, J.Z., 2015. Sources of humic-like substances in the Pearl River Delta, China: positive matrix factorization analysis of $PM_{2.5}$ major components and source markers. Atmos. Chem. Phys. 15, 1995–2008. https://doi.org/10.5194/acp-15-1995-2015.
Lambe, A.T., Avery, A.M., Bhattacharyya, N., Wang, D.Y., Modi, M., Masoud, C.G., et al., 2022. Comparison of secondary organic aerosol generated from the oxidation of laboratory precursors by hydroxyl radicals, chlorine atoms, and bromine atoms in an oxidation flow reactor. Environ. Sci.: Atmos. 2, 687–701. https://doi.org/10.1039/d2ea00018k.
Lee, H.J., Laskin, A., Laskin, J., Nizkorodov, S.A., 2013. Excitation-emission spectra and fluorescence quantum yields for fresh and aged biogenic secondary organic aerosols. Environ. Sci. Technol. 47, 5763–5770. https://doi.org/10.1021/es400644c.
Li, J.J., Zhang, Q., Wang, G.H., Li, J., Wu, C., Liu, L., et al., 2020a. Optical properties and molecular compositions of water-soluble and water-insoluble brown carbon (BrC) aerosols in Northwest China. Atmos. Chem. Phys. 20, 4889–4904. https://doi.org/10.5194/acp-20-4889-2020.
Li, X.R., Yang, Y., Liu, S.Q., Zhao, Q., Wang, G.H., Wang, Y.S., 2020b. Light absorption properties of brown carbon (BrC) in autumn and winter in Beijing: composition, formation and contribution of nitrated aromatic compounds. Atmos. Environ. 223, 117289. https://doi.org/10.1016/j.atmosenv.2020.117289.
Li, X., Yu, F., Cao, J., Fu, P., Hua, X., Chen, Q., et al., 2022. Chromophoric dissolved organic carbon cycle and its molecular compositions and optical properties in precipitation in the Guanzhong basin, China. Sci. Total Environ. 814, 152775. https://doi.org/10.1016/j.scitotenv.2021.152775.
Li, R., Zhang, M., Du, Y., Wang, G., Shang, C., Liu, Y., et al., 2023. Impacts of dust events on chemical characterization and associated source contributions of atmospheric particulate matter in northern China. Environ. Pollut. 316, 120597. https://doi.org/10.1016/j.envpol.2022.120597.
Liao, J., Huey, L.G., Tanner, D.J., Flocke, F.M., Orlando, J.J., Neuman, J.A., et al., 2012. Observations of inorganic bromine (HOBr, BrO, and Br_2) speciation at Barrow, Alaska, in spring 2009. J. Geophys. Res. - Atmos. 117, n/a. https://doi.org/10.1029/2011jd016641.
Lin, P., Hu, M., Deng, Z., Slanina, J., Han, S., Kondo, Y., et al., 2009. Seasonal and diurnal variations of organic carbon in $PM_{2.5}$ in Beijing and the estimation of secondary organic carbon. J. Geophys. Res. - Atmos., 114 https://doi.org/10.1029/2008jd010902.
Lin, P., Rincon, A.G., Kalberer, M., Yu, J.Z., 2012. Elemental composition of HULIS in the Pearl River Delta region, China: results inferred from positive and negative electrospray high resolution mass spectrometric data. Environ. Sci. Technol. 46, 7454–7462. https://doi.org/10.1021/es300285d.
Lin, P., Liu, J., Shilling, J.E., Kathmann, S.M., Laskin, J., Laskin, A., 2015. Molecular characterization of brown carbon (BrC) chromophores in secondary organic aerosol generated from photo-oxidation of toluene. Phys. Chem. Chem. Phys. 17, 23312–23325. https://doi.org/10.1039/c5cp02563j.
Liu, J., Mo, Y., Ding, P., Li, J., Shen, C., Zhang, G., 2018. Dual carbon isotopes (^{14}C and ^{13}C) and optical properties of WSOC and HULIS-C during winter in Guangzhou, China. Sci. Total Environ. 633, 1571–1578. https://doi.org/10.1016/j.scitotenv.2018.03.293.
Liu, X.Y., Zhang, Y.L., Peng, Y.R., Xu, L.L., Zhu, C.M., Cao, F., et al., 2019. Chemical and optical properties of carbonaceous aerosols in Nanjing, eastern China: regionally transported biomass burning contribution. Atmos. Chem. Phys. 19, 11213–11233. https://doi.org/10.5194/acp-19-11213-2019.
Mo, Y., Li, J., Jiang, B., Su, T., Geng, X., Liu, J., et al., 2018. Sources, compositions, and optical properties of humic-like substances in Beijing during the 2014 APEC summit: results from dual carbon isotope and Fourier-transform ion cyclotron resonance mass spectrometry analyses. Environ. Pollut. 239, 322–331. https://doi.org/10.1016/j.envpol.2018.04.041.
Mo, Y.Z., Zhong, G.C., Li, J., Liu, X., Jiang, H.X., Tang, J., et al., 2022. The sources, molecular compositions, and light absorption properties of water-soluble organic carbon in marine aerosols from South China Sea to the eastern Indian Ocean. J. Geophys. Res. - Atmos. 127. https://doi.org/10.1029/2021JD036168.
Muñiz-Unamunzaga, M., Borge, R., Sarwar, G., Gantt, B., de la Paz, D., Cuevas, C.A., et al., 2018. The influence of ocean halogen and sulfur emissions in the air quality of a coastal megacity: the case of Los Angeles. Sci. Total Environ. 610-611, 1536–1545. https://doi.org/10.1016/j.scitotenv.2017.06.098.
Ng, N.L., Kwan, A.J., Surratt, J.D., Chan, A.W.H., Chhabra, P.S., Sorooshian, A., et al., 2008. Secondary organic aerosol (SOA) formation from reaction of isoprene with nitrate radicals (NO_3). Atmos. Chem. Phys. 8, 4117–4140. https://doi.org/10.5194/acp-8-4117-2008.
Olson, M.R., Garcia, M.V., Robinson, M.A., Van Rooy, P., Dietenberger, M.A., Bergin, M., et al., 2015. Investigation of black and brown carbon multiple-wavelength-dependent light absorption from biomass and fossil fuel combustion source emissions. J. Geophys. Res. - Atmos. 120, 6682–6697. https://doi.org/10.1002/2014jd022970.
Perraud, V., Bruns, E.A., Ezell, M.J., Johnson, S.N., Greaves, J., Finlayson-Pitts, B.J., 2010. Identification of organic nitrates in the NO_3 radical initiated oxidation of α-pinene by atmospheric pressure chemical ionization mass spectrometry. Environ. Sci. Technol. 44, 5887–5893. https://doi.org/10.1021/es1005658.
Qin, J.J., Zhang, L.M., Zhou, X.M., Duan, J.C., Mu, S.T., Xiao, K., et al., 2018. Fluorescence fingerprinting properties for exploring water-soluble organic compounds in $PM_{2.5}$ in an industrial city of Northwest China. Atmos. Environ. 184, 203–211. https://doi.org/10.1016/j.atmosenv.2018.04.049.
Rai, P., Furger, M., Slowik, J.G., Zhong, H., Tong, Y., Wang, L., et al., 2021. Characteristics and sources of hourly elements in PM_{10} and $PM_{2.5}$ during wintertime in Beijing. Environ. Pollut. 278, 116865. https://doi.org/10.1016/j.envpol.2021.116865.
Riva, M., Tomaz, S., Cui, T., Lin, Y.H., Perraudin, E., Gold, A., et al., 2015. Evidence for an unrecognized secondary anthropogenic source of organosulfates and sulfonates: gas-phase oxidation of polycyclic aromatic hydrocarbons in the presence of sulfate aerosol. Environ. Sci. Technol. 49, 6654–6664. https://doi.org/10.1021/acs.est.5b00836.
Salma, I., Meszaros, T., Maenhaut, W., Vass, E., Majer, Z., 2010. Chirality and the origin of atmospheric humic-like substances. Atmos. Chem. Phys. 10, 1315–1327. https://doi.org/10.5194/acp-10-1315-2010.
Satish, R., Shamjad, P., Thamban, N., Tripathi, S., Rastogi, N., 2017. Temporal characteristics of brown carbon over the central Indo-Gangetic Plain. Environ. Sci. Technol. 51, 6765–6772. https://doi.org/10.1021/acs.est.7b00734.
Seinfeld, J.H., Bretherton, C., Carslaw, K.S., Coe, H., DeMott, P.J., Dunlea, E.J., et al., 2016. Improving our fundamental understanding of the role of aerosol-cloud interactions in the climate system. Proc. Natl. Acad. Sci. U. S. A. 113, 5781–5790. https://doi.org/10.1073/pnas.1514043113.
Shen, Z.X., Zhang, Q., Cao, J.J., Zhang, L.M., Lei, Y.L., Huang, Y., et al., 2017. Optical properties and possible sources of brown carbon in $PM_{2.5}$ over Xi'an, China. Atmos. Environ. 150, 322–330. https://doi.org/10.1016/j.atmosenv.2016.11.024.
Singh, H.B., Kasting, J.F., 1988. Chlorine-hydrocarbon photochemistry in the marine troposphere and lower stratosphere. J. Atmos. Chem. 7, 261–285. https://doi.org/10.1007/bf00130933.
Soleimanian, E., Mousavi, A., Taghvaee, S., Shafer, M.M., Sioutas, C., 2020. Impact of secondary and primary particulate matter (PM) sources on the enhanced light absorption by brown carbon (BrC) particles in Central Los Angeles. Sci. Total Environ. 705, 135902. https://doi.org/10.1016/j.scitotenv.2019.135902.
Song, J., Li, M., Jiang, B., Wei, S., Fan, X., Peng, P., 2018. Molecular characterization of water-soluble humic like substances in smoke particles emitted from combustion of biomass materials and coal using ultrahigh-resolution electrospray ionization Fourier transform ion cyclotron resonance mass spectrometry. Environ. Sci. Technol. 52, 2575–2585. https://doi.org/10.1021/acs.est.7b06126.
Song, J., Li, M., Fan, X., Zou, C., Zhu, M., Jiang, B., et al., 2019. Molecular characterization of water- and methanol-soluble organic compounds emitted from residential coal combustion using ultrahigh-resolution electrospray ionization Fourier Transform Ion Cyclotron Resonance Mass Spectrometry. Environ. Sci. Technol. 53, 13607–13617. https://doi.org/10.1021/acs.est.9b04331.
Spicer, C.W., Chapman, E.G., Finlayson-Pitts, B.J., Plastridge, R.A., Hubbe, J.M., Fast, J.D., et al., 1998. Unexpectedly high concentrations of molecular chlorine in coastal air. Nature 394, 353–356. https://doi.org/10.1038/28584.
Srinivas, B., Rastogi, N., Sarin, M.M., Singh, A., Singh, D., 2016. Mass absorption efficiency of light absorbing organic aerosols from source region of paddy-residue burning emissions in the Indo-Gangetic Plain. Atmos. Environ. 125, 360–370. https://doi.org/10.1016/j.atmosenv.2015.07.017.
Stedmon, C.A., Bro, R., 2008. Characterizing dissolved organic matter fluorescence with parallel factor analysis: a tutorial. Limnol. Oceanogr. Methods 6, 572–579. https://doi.org/10.4319/lom.2008.6.572.
Stein, A.F., Draxler, R.R., Rolph, G.D., Stunder, B.J.B., Cohen, M.D., Ngan, F., 2015. Noaa's hysplit atmospheric transport and dispersion modeling system. Bull. Am. Meteorol. Soc. 96, 2059–2077. https://doi.org/10.1175/Bams-D-14-00110.1.
Su, S.H., Xie, Q.R., Smith, A.J., Lang, Y.C., Hu, W., Cao, D., et al., 2022. A new structural classification scheme for dissolved organic sulfur in urban snow from North China. Environmental Science & Technology Letters 9, 366–374. https://doi.org/10.1021/acs.estlett.2c00153.
Surratt, J.D., Gomez-Gonzalez, Y., Chan, A.W., Vermeylen, R., Shahgholi, M., Kleindienst, T.E., et al., 2008. Organosulfate formation in biogenic secondary organic aerosol. J. Phys. Chem. A 112, 8345–8378. https://doi.org/10.1021/jp802310p.
Tanaka, P.L., Riemer, D.D., Chang, S.H., Yarwood, G., McDonald-Buller, E.C., Apel, E.C., et al., 2003. Direct evidence for chlorine-enhanced urban ozone formation in Houston, Texas. Atmos. Environ. 37, 1393–1400. https://doi.org/10.1016/S1352-2310(02)01007-5.
Tang, J., Li, J., Su, T., Han, Y., Mo, Y.Z., Jiang, H.X., et al., 2020. Molecular compositions and optical properties of dissolved brown carbon in biomass burning, coal combustion, and vehicle emission aerosols illuminated by excitation-emission matrix spectroscopy and Fourier transform ion cyclotron resonance mass spectrometry analysis. Atmos. Chem. Phys. 20, 2513–2532. https://doi.org/10.5194/acp-20-2513-2020.
Tang, J., Wang, J.Q., Zhong, G.C., Jiang, H.X., Mo, Y.Z., Zhang, B.L., et al., 2021. Measurement report: long-emission-wavelength chromophores dominate the light absorption of

brown carbon in aerosols over Bangkok: impact from biomass burning. Atmos. Chem. Phys. 21, 11337–11352. https://doi.org/10.5194/acp-21-11337-2021.
Tao, S., Lu, X., Levac, N., Bateman, A.P., Nguyen, T.B., Bones, D.L., et al., 2014. Molecular characterization of organosulfates in organic aerosols from Shanghai and Los Angeles urban areas by nanospray-desorption electrospray ionization high-resolution mass spectrometry. Environ. Sci. Technol. 48, 10993–11001. https://doi.org/10.1021/es5024674.
Teich, M., van Pinxteren, D., Wang, M., Kecorius, S., Wang, Z.B., Muller, T., et al., 2017. Contributions of nitrated aromatic compounds to the light absorption of water-soluble and particulate brown carbon in different atmospheric environments in Germany and China. Atmos. Chem. Phys. 17, 1653–1672. https://doi.org/10.5194/acp-17-1653-2017.
Tolis, E.I., Saraga, D.E., Lytra, M.K., Papathanasiou, A.C., Bougaidis, P.N., Prekas-Patronakis, O.E., et al., 2015. Concentration and chemical composition of $PM_{2.5}$ for a one-year period at Thessaloniki, Greece: a comparison between city and port area. Atmos. Environ. 113, 197–207. https://doi.org/10.1016/j.atmosenv.2015.05.014.
Wan, Y., Huang, X., Xing, C., Wang, Q., Ge, X., Yu, H., 2022. Chemical characterization of organic compounds involved in iodine-initiated new particle formation from coastal macroalgal emission. Atmos. Chem. Phys. 22, 15413–15423. https://doi.org/10.5194/acp-22-15413-2022.
Wang, L., Arey, J., Atkinson, R., 2005. Reactions of chlorine atoms with a series of aromatic hydrocarbons. Environ. Sci. Technol. 39, 5302–5310. https://doi.org/10.1021/es0479437.
Wang, Y.J., Hu, M., Wang, Y.C., Li, X., Fang, X., Tang, R.Z., et al., 2020. Comparative study of particulate organosulfates in contrasting atmospheric environments: field evidence for the significant influence of anthropogenic sulfate and NO_x. Environmental Science & Technology Letters 7, 787–794. https://doi.org/10.1021/acs.estlett.0c00550.
Wang, Y., Tong, R., Yu, J.Z., 2021a. Chemical synthesis of multifunctional air pollutants: terpene-derived nitrooxy organosulfates. Environ. Sci. Technol. 55, 8573–8582. https://doi.org/10.1021/acs.est.1c00348.
Wang, Y., Zhao, Y., Wang, Y.C., Yu, J.Z., Shao, J.Y., Liu, P., et al., 2021b. Organosulfates in atmospheric aerosols in Shanghai, China: seasonal and interannual variability, origin, and formation mechanisms. Atmos. Chem. Phys. 21, 2959–2980. https://doi.org/10.5194/acp-21-2959-2021.
Weber, R.J., Sullivan, A.P., Peltier, R.E., Russell, A., Yan, B., Zheng, M., et al., 2007. A study of secondary organic aerosol formation in the anthropogenic-influenced southeastern United States. J. Geophys. Res. - Atmos. 112. https://doi.org/10.1029/2007jd008408.
Wen, H., Zhou, Y., Xu, X., Wang, T., Chen, Q., Chen, Q., et al., 2021. Water-soluble brown carbon in atmospheric aerosols along the transport pathway of Asian dust: optical properties, chemical compositions, and potential sources. Sci. Total Environ. 789, 147971. https://doi.org/10.1016/j.scitotenv.2021.147971.
Wu, G., Ram, K., Fu, P., Wang, W., Zhang, Y., Liu, X., et al., 2019. Water-soluble brown carbon in atmospheric aerosols from Godavari (Nepal), a regional representative of South Asia. Environ. Sci. Technol. 53, 3471–3479. https://doi.org/10.1021/acs.est.9b00596.
Wu, G., Fu, P., Ram, K., Song, J., Chen, Q., Kawamura, K., et al., 2021. Fluorescence characteristics of water-soluble organic carbon in atmospheric aerosol. Environ. Pollut. 268, 115906. https://doi.org/10.1016/j.envpol.2020.115906.
Xie, M., Mladenov, N., Williams, M.W., Neff, J.C., Wasswa, J., Hannigan, M.P., 2016. Water soluble organic aerosols in the Colorado Rocky Mountains, USA: composition, sources and optical properties. Sci. Rep. 6, 39339. https://doi.org/10.1038/srep39339.
Xie, X., Chen, Y., Nie, D., Liu, Y., Liu, Y., Lei, R., et al., 2020. Light-absorbing and fluorescent properties of atmospheric brown carbon: a case study in Nanjing, China. Chemosphere 251, 126350. https://doi.org/10.1016/j.chemosphere.2020.126350.
Yan, C.Q., Zheng, M., Sullivan, A.P., Bosch, C., Desyaterik, Y., Andersson, A., et al., 2015. Chemical characteristics and light-absorbing property of water-soluble organic carbon in Beijing: biomass burning contributions. Atmos. Environ. 121, 4–12. https://doi.org/10.1016/j.atmosenv.2015.05.005.
Yan, C.Q., Zheng, M., Bosch, C., Andersson, A., Desyaterik, Y., Sullivan, A.P., et al., 2017. Important fossil source contribution to brown carbon in Beijing during winter. Sci. Rep. 7, 43182. https://doi.org/10.1038/srep43182.
Yu, Z., Li, Y., 2021. Marine volatile organic compounds and their impacts on marine aerosol-a review. Sci. Total Environ. 768, 145054. https://doi.org/10.1016/j.scitotenv.2021.145054.
Yu, G.H., Park, S., Shin, S.K., Lee, K.H., Nam, H.G., 2018. Enhanced light absorption due to aerosol particles in ship plumes observed at a seashore site. Atmos. Pollut. Res. 9, 1177–1183. https://doi.org/10.1016/j.apr.2018.05.005.
Yuan, W., Huang, R.J., Yang, L., Guo, J., Chen, Z.Y., Duan, J., et al., 2020. Characterization of the light-absorbing properties, chromophore composition and sources of brown carbon aerosol in Xi'an, northwestern China. Atmos. Chem. Phys. 20, 5129–5144. https://doi.org/10.5194/acp-20-5129-2020.
Zhang, J., Yuan, Q., Liu, L., Wang, Y.Y., Zhang, Y.X., Xu, L., et al., 2021. Trans-regional transport of haze particles from the North China Plain to Yangtze River Delta during winter. J. Geophys. Res. - Atmos. 126. https://doi.org/10.1029/2020JD033778.
Zhang, L.Y., Son, J.H., Bai, Z., Zhang, W., Li, L., Wang, L.N., et al., 2022. Characterizing atmospheric brown carbon and its emission sources during wintertime in Shanghai, China. Atmosphere 13, 991. https://doi.org/10.3390/atmos13060991.
Zhou, J., Ho, S.S.H., Cao, J., Zhao, Z., Zhao, S., Zhu, C., et al., 2018. Chemical characterization of $PM_{2.5}$ from a southern coastal city of China: applications of modeling and chemical tracers in demonstration of regional transport. Environ. Sci. Pollut. Res. 25, 20591–20605. https://doi.org/10.1007/s11356-018-2238-1.
Zhou, R., Yan, C., Yang, Q., Niu, H., Liu, J., Xue, F., et al., 2023. Characteristics of wintertime carbonaceous aerosols in two typical cities in Beijing-Tianjin-Hebei region, China: Insights from multiyear measurements. Environ. Res. 216, 114469. https://doi.org/10.1016/j.envres.2022.114469.
Ziemann, P.J., Atkinson, R., 2012. Kinetics, products, and mechanisms of secondary organic aerosol formation. Chem. Soc. Rev. 41, 6582–6605. https://doi.org/10.1039/c2cs35122f.